The Astrophysical Journal, 701:1091–1115, 2009 August 20 doi:10.1088/0004-637X/701/2/1091

A FAR ULTRAVIOLET SPECTROSCOPIC EXPLORER SURVEY OF HIGH-DECLINATION DWARF NOVAE*

Patrick Godon[1,4], Edward M. Sion[1], Paul E. Barrett[2], and Paula Szkody[3]
[1] Department of Astronomy and Astrophysics Villanova University, Villanova, PA 19085, USA; patrick.godon@villanova.edu, edward.sion@villanova.edu
[2] United States Naval Observatory, Washington, DC 20392, USA; barrett.paul@usno.navy.mil
[3] Department of Astronomy, University of Washington, Seattle, WA 98195, USA; szkody@astro.washington.edu
Received 2009 January 12; accepted 2009 June 19; published 2009 July 29

ABSTRACT

We present a spectral analysis of the *Far Ultraviolet Spectroscopic Explorer* (*FUSE*) spectra of eight high-declination dwarf novae (DNs) obtained from a Cycle 7 *FUSE* survey. These DN systems have not been previously studied in the UV and little is known about their white dwarfs (WDs) or accretion disks. We carry out the spectral analysis of the *FUSE* data using synthetic spectra generated with the codes TLUSTY and SYNSPEC. For two faint objects (AQ Men and V433 Ara) we can only assess a lower limit for the WD temperature or mass accretion rate. NSV 10934 was caught in a quiescent state and its spectrum is consistent with a low-mass accretion rate disk. For five objects (HP Nor, DT Aps, AM Cas, FO Per, and ES Dra), we obtain WD temperatures between 34,000 K and 40,000 K and/or mass accretion rates consistent with intermediate to outburst states. These temperatures reflect the heating of the WD due to on-going accretion and are similar to the temperatures of other DNs observed on the rise to, and in decline from outburst. The WD temperatures we obtain should therefore be considered as upper limits, and it is likely that during quiescence AM Cas, FO Per, and ES Dra are near the average WD $T_{\rm eff}$ for catalcysmic variables above the period gap (∼30,000 K), similar to U Gem, SS Aur, and RX And.

Key words: stars: dwarf novae – white dwarfs

Online-only material: color figures

1. INTRODUCTION

1.1. Cataclysmic Variables

Cataclysmic variables (CVs) are semidetached binary systems, in which a white dwarf star (WD) accretes matter from a main-sequence (MS or post-MS; the *secondary*) star. Accretion takes place via a disk for nonmagnetic WDs and via a column or curtain for magnetic WDs (for a review on CVs, see Hack & La Dous 1993; Warner 1995). The luminosity of a CV can vary significantly, and systems can be found in a state of low luminosity (*quiescence*), high luminosity (*outburst*), or even in a rather *intermediate* state when the system is *active* without reaching its peak luminosity (Robinson 1976; Hack & La Dous 1993; Warner 1995). CVs are divided in subclasses according to the duration, occurrence and amplitude of their outbursts.

The two main types of CVs are dwarf nova (DN) and nova-like (NL) systems. Dwarf novae are weakly or nonmagnetic disk systems divided into U Gem systems, SU UMa systems, and Z Cam systems. The U Gem systems are the typical DNs, i.e., those systems exhibiting normal DN outbursts; the SU UMas exhibit both normal DN outbursts and superoutbursts, which are both longer in duration and higher in luminosity than normal DN outbursts; and the Z Cam systems have standstills where they remain in a semi-outburst state for a long time. Nova-likes form a less homogeneous class, e.g., nonmagnetic disk systems found mostly in high state (known anti-DN or VY Scl) systems that exhibit no known low states (UX UMa systems), nondisk magnetic systems (AM Her stars or Polars), magnetic systems with truncated disk (Intermediate Polars), etc. See, e.g., Ritter & Kolb (2003) for the classification of CVs.

The binary orbital period in CVs ranges from a fraction of an hour to about a day; however, there is a gap in the orbital period between 2 and 3 hr where almost no CV systems are found (hereafter the "period gap"; Whyte & Eggleton 1980). The U Gem and Z Cam DN systems are found above the period gap, while the SU UMa DN systems are found below the period gap.

1.2. The Standard Model

In the commonly accepted (standard) theory of evolution of CVs, systems evolve through the gap from long periods to shorter periods, driven by angular momentum loss. Above the gap ($P > 3$ hr) magnetic braking (Weber & Davis 1967; Verbunt & Zwaan 1981) is thought to be the dominant mechanism for angular momentum loss due to wind loss of the tidally locked secondary. At about $P \approx 3$ hr, magnetic braking stops when the secondary becomes fully convective, and its radius becomes smaller than the Roche lobe radius: the secondary detaches from the Roche lobe. At this point, gravitational radiation (Faulkner 1971; Paczyński & Sienkiewicz 1981; Rappaport et al. 1982) is believed to take over as the main mechanism for angular momentum loss. The binary separation and period keep on decreasing until $P \approx 2$ hr, at which time the Roche lobe radius again becomes comparable to the radius of the secondary, and the binary again becomes a contact binary. The disrupted (or *interrupted*) magnetic braking became the standard scenario of CV evolution explaining the presence of the period gap around 3 hr (Paczyński & Sienkiewicz 1983; Rappaport et al. 1983; Spruit & Ritter 1983; Hameury et al. 1988; King 1988; Kolb 1993; Howell et al. 2001).

The first comparison of CV WD temperatures with actual evolutionary tracks (the evolutionary tracks of Mc Dermott & Taam 1989) was carried out by Sion (1991), who compared the CV WD $T_{\rm eff}$ values as a function of orbital period with the cooling curves of nonaccreting WDs and with the theoretical prediction of $\dot{M}$ (hence $T_{\rm eff}$) versus P of Mc Dermott & Taam

* Based on observations made with the NASA–CNES–CSA Far Ultraviolet Spectroscopic Explorer. *FUSE* is operated for NASA by the Johns Hopkins University under NASA contract NAS5-32985.
[4] Visiting at the Space Telescope Science Institute, Baltimore, MD 21218, USA; godon@stsci.edu.

Report Documentation Page

Form Approved
OMB No. 0704-0188

1. REPORT DATE	2. REPORT TYPE	3. DATES COVERED
20 AUG 2009		**00-00-2009 to 00-00-2009**

4. TITLE AND SUBTITLE	5a. CONTRACT NUMBER
A Far Ultraviolet Spectroscopic Explorer Survey of HIgh-Declination DWARF NOVAE	5b. GRANT NUMBER
	5c. PROGRAM ELEMENT NUMBER
6. AUTHOR(S)	5d. PROJECT NUMBER
	5e. TASK NUMBER
	5f. WORK UNIT NUMBER
7. PERFORMING ORGANIZATION NAME(S) AND ADDRESS(ES) **Department of Astronomy and Astrophysics Villanova University,Villanova,PA,19085**	8. PERFORMING ORGANIZATION REPORT NUMBER
9. SPONSORING/MONITORING AGENCY NAME(S) AND ADDRESS(ES)	10. SPONSOR/MONITOR'S ACRONYM(S)
	11. SPONSOR/MONITOR'S REPORT NUMBER(S)

12. DISTRIBUTION/AVAILABILITY STATEMENT
Approved for public release; distribution unlimited

13. SUPPLEMENTARY NOTES

14. ABSTRACT

15. SUBJECT TERMS

16. SECURITY CLASSIFICATION OF:			17. LIMITATION OF ABSTRACT	18. NUMBER OF PAGES	19a. NAME OF RESPONSIBLE PERSON
a. REPORT **unclassified**	b. ABSTRACT **unclassified**	c. THIS PAGE **unclassified**	**Same as Report (SAR)**	**25**	

(1989). Sion (1991) found some evidence, though far from conclusive, that CV systems evolve across the period gap. However, the standard model is based on an ad hoc assumption about the mechanism of orbital angular momentum loss, and many of its predictions are in disagreement with the observations (Townsley & Gänsicke 2009). For example, if CVs are evolving from longer period to shorter period across the gap, then short period DNs are older and with a longer history of angular momentum transfer via disk accretion, and their WDs should rotate faster than DN WDs above the gap. However, so far, there is no observational evidence pointing to this. Modifications have been proposed to the standard model (Basri 1987; Hameury et al. 1990; McCormick & Frank 1998; Schenker et al. 1998; Kolb & Baraffe 1999; Clemens et al. 1998; Spruit & Taam 2001; Taam & Spruit 2001; Kolb et al. 2001; King et al. 2002; Taam et al. 2003; Ivanova & Taam 2004). One of the alternatives has been the suggestion that CVs above and below the gap form two distinct populations not related to each other (Eggleton 1976; Webbink 1981; Andronov N. et al. 2003).

In order to put more constraints on the theories of the evolution of CVs, more observations are needed (Sion 1991; Gänsicke 2005). The standard model gives a prediction of $\dot{M}$ above the period gap (as a function of the binary period) and as a consequence $\dot{M}$ is the most important parameter to test the theory. Unfortunately, to derive $\dot{M}$ from observations proves to be difficult, as it itself relies on many unknowns (e.g., the distance). For example, optical observations seem to indicate that $\dot{M}$ is correlated with the period (Patterson 1984), while FUV spectroscopy (albeit of NLs alone) does not show any correlation at all (Puebla et al. 2007).

1.3. The White Dwarf Temperature: The Case for Dwarf Novae

Recently, Townsley & Bildsten (2003, 2004) have shown that the quiescent effective temperatures $T_{\rm eff}$ of the WD in CVs approaches an equilibrium value when the WD is subject to accretion at an average accretion rate $\dot{M}$ which is constant on time scales similar to the WD core thermal time (∼100 Myr). This equilibrium value is a function of the WD mass and mass accretion rate only. Therefore, the knowledge of the quiescent surface temperature of the WD and its mass can be used to obtain an estimate of the average mass accretion rate (it seems counterintuitive that the effective temperature of the WD would not depend on its age; the limitations and the applications of the relation between $< \dot{M} >$ and $T_{\rm eff}$ are discussed by Townsley & Gänsicke 2009). As a consequence, CV WD temperature has become the most important observational parameter, together with the binary period and WD mass, to test the theories of the evolution of CVs.

For DNs below the gap, the distribution of WD temperatures obtained from FUV spectroscopic analysis seems to be centered around T_{wd} ∼15,000 K, while for systems above the gap the WD temperatures are higher, somewhere between ∼30,000 K and up to ∼50,000 K (Sion et al. 2008). Above the gap at periods of about 200–300 minutes, the WDs in DNs are about 10,000 K cooler than the WDs in VY Scl systems (Godon et al. 2008b). On the other hand, polars (devoid of disks) have the coolest WDs of all, with $T_{wd} < 20{,}000$ K above the gap and $T < 15{,}000$ K below the gap (Araujo-Betancor et al. 2005; see Townsley & Gänsicke 2009, for a review of WD temperatures in CVs).

Currently, the number of white dwarf temperatures known is as follows. There are 10 NL AM Her systems below the gap and three above the gap; five NL VY Scl systems above the gap; 19 DN SU UMa systems below the gap; 12 DN U Gem systems above the gap; and only two DN Z Cam systems above the gap. There is a critical shortage in knowledge of the WD effective temperature $T_{\rm eff}$ for DN Z Cam, NL AM Her, and NL VY Scl all above the period gap. Thus, detailed comparisons of accreting WDs above and below the gap cannot be made.

However, during quiescence DNs, unlike other CVs, have the advantage of exposing their WD in the FUV for long periods of time. With a temperature range ∼12,000–50,000 K, the WD peaks in the FUV, and this makes *FUSE* the best instrument to observe the WD of quiescent DNs. Furthermore, DNs offer a fairly reliable estimate of their distances via the absolute magnitude at maximum versus orbital period relation found by Warner (1987) and Harrison et al. (2004). As a consequence, DNs are ideal candidates to observe with *FUSE*, as one can more easily derive the WD temperature.

More precisely, by fitting the observed quiescent spectrum with synthetic spectra, one can, in theory, derive the WD parameters such as the temperature, gravity, rotational velocity, and chemical abundances (mainly for C, N, S, Si). The (instantaneous) mass accretion rate of many systems can also be deduced at given epochs of outburst or quiescence using spectral fitting techniques of FUV spectra. In practice, however, to obtain robust results in the spectral analysis and depending on the quality of the observed spectrum, one needs to know the distance d to the system, the WD mass M_{wd}, and possibly also the inclination of the system (see Sections 3 and 4).

For these reasons, we present here a spectroscopic analysis of a sample of dwarf novae from our Cycle 7 *FUSE* survey. The present analysis includes eight dwarf nova systems: five systems above the gap (including four Z Cam), one below the gap, and two with unknown period. The observations are described in the next section, including the details of the processing of the spectra and a general description of the lines seen in *FUSE* spectra of DNs. In Section 3, we present our synthetic spectral modeling that we use to analyze the spectra. In Section 4, we present and discuss the results of the spectral analysis for each system separately. And in the last section we give a summary of our findings.

2. OBSERVATIONS

2.1. The FUSE Spectra

The *FUSE* targets are listed in Table 1 with their system parameters as follows: Column (1) name, (2) CV subtype, (3) orbital period in days, (4) orbital inclination in degrees, (5) apparent magnitude in outburst, (6) apparent magnitude in quiescence, and (7) priority given as a *FUSE* target (1 = high, 2 = low).

The observation log is presented in Table 2. The following systems were also listed as targets in our original proposal, but they were not observed with *FUSE*: AD Men, V342 Cen, V1040 Cen, and TZ Per. From the *AAVSO* (American Association of Variable Stars Observers) data (Price 2006), we were able to assess the state of each target at the time of the *FUSE* observations.

All the *FUSE* spectra were obtained through the 30"× 30" LWRS Large Square Aperture in TIME TAG mode. The data were processed with the latest and final version of CalFUSE (v3.2.0; for more details, see Dixon et al. 2007). The *FUSE* data come in the form of eight spectral segments (SiC1a, SiC1b, SiC2a, SiC2b, LiF1a, LiF1b, LiF2a, and LiF2b), which are combined together to give the final *FUSE* spectrum. To process *FUSE* data, we follow the same procedure we used previously

Table 1
System Parameters of the *FUSE* Targets

Name[a]	Type	P_{orb} (hr)	i (deg)	V_{max}	V_{min}	Priority
VW Tuc	UG	···	>20?	15.2	< 16.5	2
AQ Men	UG/NL?	3.40	eclipsing	14	15	1
HP Nor	ZC	···	···	12.8	16.4	2
IK Nor	UG	···	···	12.9	16.3	2
V663 Ara	SU	···	···	15.9	< 16.3	2
V433 Ara	ZC/NL?	4.70	···	14.8	< 16.3	2
V499 Ara	UG	···	···	14.8	< 16.2	2
DT Aps	SS	···	···	14.4	< 15.8	1
NSV 10934	SU	1.74	···	11.2	15.0	1
AM Cas	ZC	3.96	···	12.3	15.2	1
FO Per	UG	3.52/4.13	···	11.8	16.2	1
ES Dra	ZC	4.29	low?	13.9	16.3	1

Note.
[a] The targets are listed in order of ascending R.A., southern hemisphere objects followed by northern hemisphere objects.

for the analysis of other systems (such as WW Ceti; Godon et al. 2006a); consequently, we give here only a short account of this procedure. The spectral regions covered by the spectral channels overlap, and these overlap regions are then used to renormalize the spectra in the SiC1, LiF2, and SiC2 channels to the flux in the LiF1 channel. We then produced a final spectrum that covers the full *FUSE* wavelength range 905–1187 Å. The low-sensitivity portions of each channel were discarded. In most channels, there exists a narrow dark stripe of decreased flux in the spectra running in the dispersion direction, known as the "worm," which can attenuate as much as 50% of the incident light in the affected portions of the spectrum; this is due to shadows thrown by the wires on the grid above the detector. In the present observations, the worm affected mainly the 1bLiF channel. Because of the temporal changes in the strength and position of the "worm," CALFUSE cannot correct target fluxes for its presence. Therefore, we carried out a visual inspection of the *FUSE* channels to locate the worm and *manually* discarded the portion of the spectrum affected by the worm. We combined the individual exposures and channels to create a time-averaged spectrum weighting the flux by the exposure time and sensitivity of the input exposure and channel of origin.

For all the targets we had to remove the edges of the SiC channels and the worm (∼1140–1180 Å) in the 1bLiF channel. In some cases, we had to remove entire channels due to their very poor signal-to-noise ratio (S/N). Specifically, we proceeded as follows:
1. AQ Men, we kept only the 2aLif and 2bLif channels;
2. HP Nor, we removed all the SiC channels while keeping the LiF channels;
3. DT Aps, we removed large portions (at the edges) of the SiC channels;
4. AM Cas, we discarded the 2bLiF, 2bSiC, 2aLiF, and 2aSic channels and only used 1aSiC, 1bSiC, 1aLiF, and 1bLiF;
5. NSV 10934, we removed 1aSic, 2bSiC, 2bLiF;
6. FO Per, we kept all the channels;
7. ES Dra, we kept all the channels; and
8. V433 Ara, all the SiC channels were discarded and only the LiF channels were kept.

2.2. The FUSE Lines

The main emitting components contributing to the *FUSE* spectra of DNs are the accretion disk and the WD: the disk dominates during outburst, while the WD dominates during quiescence. The main feature of the spectra is the broad Lyβ absorption feature, which can be easily used to assess the gravity and the temperature of the emitting gas. At higher temperatures, as the continuum rises in the shorter wavelengths, the higher orders of the Lyman series also become visible; however, they become narrower.

Additional broad absorption lines of metals (C, S, Si) are detected and help to determine the chemical abundances and projected rotational velocity of the emitting gas. In the present spectra, the main absorption features observed are C II (1010 Å), C III (1175 Å), Si III (≈1108–1114 Å and ≈1140–1144 Å), Si IV (≈1067 Å and ≈1120–1130 Å), S IV (1073 Å), and N II (1085 Å when not contaminated by airglow).

On top of the spectrum, broad emission lines are also found in two of the systems, NSV 10934 and AQ Men, mainly the O VI doublet and C III (977 Å and 1175 Å). The broad emission lines in NSV 10934 and AQ Men originate from the hot accretion region on the white dwarf, and possibly also from the inner disk itself, as expected for high-inclination DNs in quiescence such as BZ UMa (Gänsicke et al. 2003) or EK TrA (Godon et al. 2008a). AQ Men is eclipsing and the presence of broad

Table 2
FUSE Observations Log

System Name	Date (yy/mm/dd)	Exp. time (s)	Data set	Aperture	Operation Mode	V	State	Data Quality
VW Tuc	2006 Jun 11	8,835	G9250101	LWRS	TTAG	16–18?	Quiescence	Unusable
AQ Men	2006 Nov 22	22,661	G9250201	LWRS	TTAG	14–15	Usual state	Poor
HP Nor	2007 Apr 13	3,952	G9250601	LWRS	TTAG	15.0	Low	Poor
IK Nor	2007 Apr 13	7,947	G9250701	LWRS	TTAG	···	···	Unusable
V663 Ara	2007 Apr 12	4,807	G9250802	LWRS	TTAG	···	···	Unusable
	2006 Apr 24	9,785	G9250801	LWRS	TTAG	···	···	Unusable
V433 Ara	2007 Feb 18	7,009	G9250901	LWRS	TTAG	···	···	Unusable
V499 Ara	2006 Jun 22	17,988	G9251001	LWRS	TTAG	···	···	Unusable
DT Aps	2006 May 3	8,053	G9251102	LWRS	TTAG	···	Decline/low	Unusable
	2006 Apr 28	68,245	G9251101	LWRS	TTAG	···	Active	Poor
NSV 10934	2006 Jun 28	11,956	G9251201	LWRS	TTAG	···	···	Poor
	2006 Jun 30	14,177	G9251202	LWRS	TTAG	···	···	Poor
AM Cas	2006 Oct 19	12,909	G9251402	LWRS	TTAG	13.3–13.8	Intermediate	Good
FO Per	2007 Feb 11	2,716	G9251501	LWRS	TTAG	13.5	Intermediate	Good
ES Dra	2006 Nov 19	24,554	G9251601	LWRS	TTAG	15.1–15.4	Intermediate	Good

emission lines in NSV 10934 might be an indication that it is a high-inclination system.

All our *FUSE* spectra show some ISM molecular hydrogen absorption. The most affected targets reveal a spectrum "sliced" at almost equal intervals (∼12 Å), starting at wavelengths around 1110 Å and continuing toward shorter wavelengths all the way down to the hydrogen cutoff around 915 Å. In the affected *FUSE* spectra, we identified the most prominent molecular hydrogen absorption lines by their band (Werner or Lyman), upper vibrational level (1–16), and rotational transition (R, P, or Q) with lower rotational state ($J = 1, 2, 3$).

In addition, the targets that are weak *FUSE* sources exhibit sharp emission lines from airglow (geo- and heliocoronal in origin; some of which is due to sunlight reflected inside the telescope), such as H I series, S VI (934, 944), O VI doublet, C III (977), and He I (1168).

For each system, we mark on the figures the lines that are detected as well as lines that are commonly seen for comparison. The lines that are commonly seen in the *FUSE* spectra of quiescent DN systems are as follows. At lower temperatures ($15{,}000\ \mathrm{K} < T < 25{,}000\ \mathrm{K}$), the observed lines are (e.g., Godon et al. 2008a), C III (1175 Å), C II (1066 Å), Si III (≈1108–1114 Å and ≈1140–1144 Å), and N II (1085 Å when not contaminated by airglow). At higher temperatures ($T > 25{,}000$ K), as the continuum rises in the shorter wavelengths, the higher orders of the Lyman series are revealed. At these temperatures the S IV (1073 Å) absorption line starts to appear, and, as there is more flux in the shorter wavelengths, the C II (1010 Å) absorption line also becomes visible (see, e.g., Urban & Sion 2006; Long & Gilliland 1999). At still higher temperature ($T > 50{,}000$ K), the C II and Si III lines disappear, and the spectrum becomes dominated by high-order ionization lines such as N IV (≈923 Å), S VI (933.5 and 944.5 Å), S IV (1063 and 1073 Å), Si IV (1066.6 Å), and O IV (1067.8 Å) (see, e.g., Hartley et al. 2005; Sion et al. 2007).

Because of the low quality of the spectra, the observed wavelengths cannot be determined accurately and, therefore, we do not list the wavelengths of the lines in a table. The lines are discussed for each object separately.

3. SPECTRAL MODELING

3.1. The Synthetic Stellar Spectral Codes

Before we carry out the actual fit for each individual observed spectrum, we create a grid of model spectra for high-gravity stellar atmospheres using codes TLUSTY and SYNSPEC[5] (Hubeny 1988; Hubeny & Lanz 1995). Atmospheric structure is computed (using TLUSTY) assuming a H–He LTE atmosphere; the other species are added in the spectrum synthesis stage using SYNSPEC. For hot models (say $T > 50{,}000$ K) we switch the approximate NLTE treatment option in SYNSPEC (this allows us to consider and approximate NLTE treatment even for LTE models generated by TLUSTY). We generate photospheric models with effective temperatures ranging from 12,000 K to 75,000 K in increments of about 10% (e.g., 1000 K for $T \approx 15{,}000$ K and 5000 K for $T \approx 70{,}000$ K). As the WD mass in these DN systems is not known, we choose values of $\mathrm{Log}(g)$ ranging between 7.5 and 9.5. We also vary the stellar rotational velocity $V_{\rm rot}\sin(i)$ from 100 km s^{-1} to 1000 km s^{-1} in steps of 100 km s^{-1}. As a default, solar abundances are assumed for all the models in the grid. We have, however, the option to vary the chemical abundances of individual elements in the models in the grid. For any WD mass, there is a corresponding radius, or equivalently, one single value of $\log(g)$ (e.g., see the mass–radius relation from Hamada & Salpeter 1961 or see Wood 1995 and Panei et al. 2000 for different composition and nonzero temperature WDs).

The same suite of code is also used to generate spectra of accretion disks (Wade & Hubeny 1998) based on the standard model of Shakura & Sunyaev (1973). In the present work, we use disk spectra from the grid of spectra generated by Wade & Hubeny (1998) as well as disk spectra that we generate. A detailed description of the procedure to generate such disk spectra is given by Wade & Hubeny (1998).

3.2. Synthetic Spectral Model Fitting

Before carrying out a synthetic spectral fit of the spectra, we masked portions of the spectra with strong emission lines, strong ISM molecular absorption lines, detector noise, and airglow. These regions of the spectra are somewhat different for each object and are not included in the fitting. The regions excluded from the fit are in blue in the figures. The excluded ISM quasimolecular absorption lines are marked with vertical labels in the figures.

After having generated grids of models for each target, we use FIT (Press et al. 1992), a χ^2 minimization routine, to compute the reduced χ^2_ν (χ^2 per number of degrees of freedom) and scale factor values for each model fit. While we use a χ^2 minimization technique, we do not blindly select the least χ^2 models, but we examine the models that best fit some of the features such as absorption lines (see the fit to the *FUSE* spectrum alone) and, when possible, the slope of the wings of the broad Lyman absorption features. When possible, we also select the models that are in agreement with the distance of the system (or its best estimate).

The flux level at 1000 Å (between Lyδ and Lyγ) is close to zero for temperatures below 18,000 K, at 30,000 K it is about 50% of the continuum level at 1100 Å and it reaches 100% for $T > 45{,}000$ K. At higher temperature ($T > 50{,}000$ K) the spectrum becomes pretty flat and there is not much difference in the shape of the spectrum between (say) a 50,000 K and a 80,000 K model. When fitting the shape of the spectrum in such a manner, an accuracy of about 500–1000 K is obtained, due to the S/N. In theory, a fine tuning of the temperature (say to an accuracy of about ±50 K) can be carried out by fitting the flux levels such that the distance to the system (if known) is matched. However, the fitting to the distance depends strongly on the radius (and therefore the mass) of the WD. In all the systems presented here, the mass of the WD and the distance are unknown and, therefore, we are unable to assess the temperature accurately. Furthermore, since the Lyβ profile depends on both the temperature and the gravity of the WD, the accuracy of the solution is further decreased as there is a degeneracy in the solution, namely the solution spreads over a region of the $\log(g)$ and T parameter space. And last, reddening values are rarely known, therefore increasing even more the inaccuracy of assessing the temperature by scaling the synthetic flux to the observed flux. As a consequence, for each target we present more than one model fit.

For DT Aps and ES Dra, we vary the abundances; however, because of the low S/N, for all the other spectra we fit solar abundance models and do not change the abundance of the species.

The WD rotation ($V_{\rm rot}\sin(i)$) rate is determined by fitting the observed *FUSE* spectrum with WD models with increasing

[5] http://nova.astro.umd.edu; TLUSTY version 200; SYNSPEC version 48.

Table 3
Parameters Adopted for the Modeling

System Name	Period (hr)	Gal. Lat. (deg)	$E^{\rm Gal}_{B-V}$	$E^{\rm adp}_{B-V}$	d_w (pc)	d_h (pc)	d_k (pc)	d (pc)
HP Nor	···	−3	0.63	0.20	···	···	···	···
DT Aps	···	−20	0.09	0.09	···	···	···	···
NSV 10934	1.74	−27	0.16	0.10	151	155	117–219	150
AQ Men	3.40	−31	0.18	0.10	664	752	201–377	710
FO Per	3.52	0	1.78	0.30	244	279	182–342	260
	4.13	0	1.78	0.30	262	311	227–311	285
AM Cas	3.96	9	0.89	0.20	324	380	153–287	350
ES Dra	4.29	47	0.02	0.00	702	840	540–1016	770
V433 Ara	4.70	−9	0.19	0.10	1114	1368	747–1411	1200
TZ Per	6.31	−3	0.78	0.27	424	575	···	500

Notes.
The systems are listed in order of increasing binary period. In column (3) we list the Galactic latitude. In column (4) we list the Galactic reddening, which is anticorrelated to the Galactic latitude. as inferred from the 100 μm dust emission map (Schlegel et al. 1998). In column (5) we list the reddening we used in our modeling. In column (6) we list the distance assessed using the period–magnitude correlation given by Warner (1987). In column (7) we list the distance assessed using the period–magnitude correlation given by Harrison et al. (2004). In column (8) we list the distance estimated using the secondary IR emission technique of Knigge (2006, 2007). In the last column we list the distance we used in our modeling. TZ Per was not observed but has been added for comparison.

values of the rotational velocity. We did not carry out separate fits to individual lines, but rather tried to fit the lines and the continuum in the same fit.

For each spectrum, when possible, we try to fit a single WD model, a single disk model, and a composite WD+disk model, assuming different reddening values. For all the systems presented here the WD mass is unknown and the distance is estimated using the maximum magnitude/period relation (Warner 1987; Harrison et al. 2004), or (when the period is unknown) the method described by (Knigge 2006, 2007; see Table 3).

For the single WD model, we vary the temperature while first keeping the WD mass constant, starting at about 0.4 $M_\odot$. Once the lowest χ^2 has been found for a given mass, we vary the projected rotational velocity, and possibly also the abundances, to further lower the χ^2 and obtain a best fit. Once the best fit has been found for that mass, we assume a slightly larger mass and again vary the temperature until the lowest χ^2 is found. We follow this procedure iteratively until we reach a mass of about 1.2 $M_\odot$. The next step is to find, from all these lowest χ^2 models, which one agrees best with the distance estimate or which one has the lowest χ^2 of all (if the constraint on the distance cannot be used). For the single disk model, we carry out a similar procedure by varying the mass accretion rate and inclination assuming discrete values of the WD mass, and then chose the least χ^2 model agreeing best with the distance. And last, we use the same procedure for the WD+disk composite modeling to find the best-fit model.

4. RESULTS AND DISCUSSION

Four systems were caught in deep quiescence, and their *FUSE* spectra have such a low S/N that they are unusable. This is not only due to the intrinsic low brightness of the targets, but also due to the loss of data in some *FUSE* channels (mainly SiC) and to the loss of good exposure time (e.g., due to jitters). These four systems are VW Tucanae/HV 6327, IK Normae, V663 Arae/S 5893, and V499 Arae/S 6115. The remaining eight systems that were successfully observed are presented here.

4.1. Southern Hemisphere Systems

4.1.1. HP Normae/HV 8865

HP Nor is a DN Z Cam system (Vogt & Bateson 1982) which exhibits coherent oscillations during outbursts with a period of ∼18.6 s (Pretorius et al. 2006). Its magnitude varies between $V = 12.6$ at maximum and $V = 16.4$ at minimum (Bruch & Engel 1994). The distance to HP Nor is not known, and since its period is also unknown, we have no way to assess its distance. HP Nor was observed with *FUSE* on April 13 (JD 2454203.7). Data from the AAVSO and AVSON imply that the system was in a low state of brightness $V \sim 15$, though it did not reach its lowest magnitude $V = 16.4$. The continuum flux level of the *FUSE* spectrum is roughly consistent with the continuum flux level in the optical around 3200 Å obtained by Munari & Zwitter (1998), who observed the system in an apparent decline from outburst with $V = 14.18$ and a flux level of 2×10^{-14} erg cm^{-2} s^{-1} Å^{-1}. The *FUSE* spectrum of HP Nor is presented in Figure 1. The reddening toward HP Nor is not known; however, the Galactic reddening in this direction is 0.63. Therefore, in the following we model HP Nor assuming both $E(B-V) = 0.0$ and $E(B-V) = 0.2$.

$E(B-V) = 0.0$. For the single WD model, assuming $M_{wd} = 0.8\,M_\odot$, we find a temperature of 37,000 K and a distance of 648 pc. The projected rotational velocity is $v_{\rm rot} \sin i = 1000$ km s^{-1} to fit the C III (1175) line profile. The χ^2 obtained is smaller than one due to the poor S/N, namely $\chi^2_\nu = 0.107$. The results are listed in Table 4, where we also present a 0.4 $M_\odot$ WD and a 1.2 $M_\odot$ WD models. For the single disk models, assuming a 0.8 $M_\odot$ WD mass, we find $\dot{M} = 10^{-9.0}\,M_\odot$ yr^{-1}, $i < 41^\circ$, $d = 1603$ pc, and $\chi^2_\nu = 0.104$. Again, in Table 4 we list the results assuming different values for M_{wd}. There is basically no difference in the quality of the fits between the disk model and the single WD model. A WD+disk composite model does not improve the fit. Because the WD mass and the distance are unknown, we are left with solutions spanning a large area in the parameter space, especially for the composite WD+disk models. We do not list the results for the composite models as there is clearly a degeneracy in the solution.

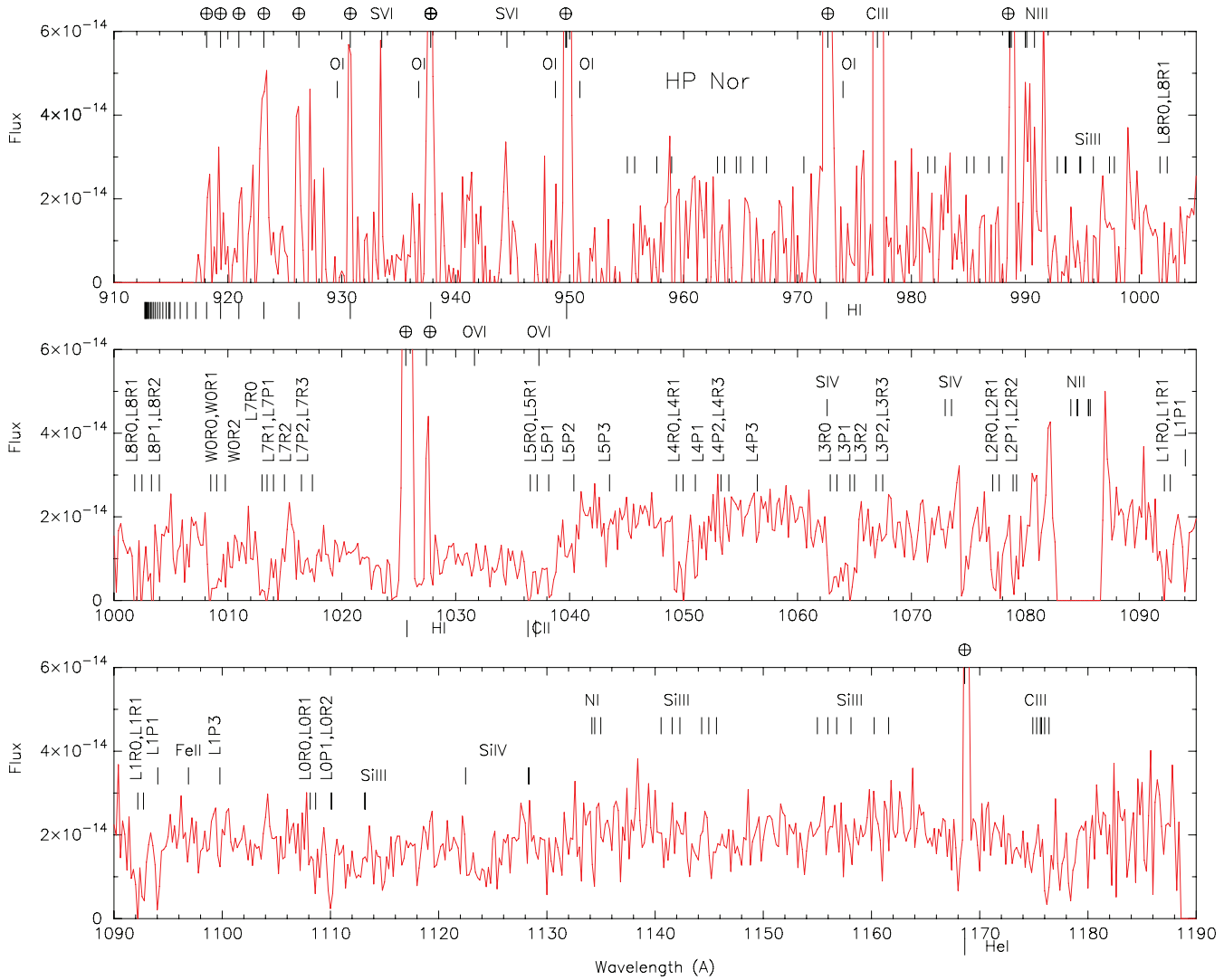

Figure 1. *FUSE* spectrum of HP Nor. The sharp emission lines (including S VI 944 Å) are due to geo- and heliocoronal contamination. The ISM molecular features are denoted for clarity. The C III (1175 Å) absorption feature is identified possibly with a redshift of ∼2 Å. The S IV (1073 Å), Si III (1113 Å), Si IV (1122 and 1128 Å) lines could also be accounted for with a redshift of ∼2 Å. Other metal lines have been marked but are not detected.

(A color version of this figure is available in the online journal.)

$E(B-V) = 0.2$. Dereddening the spectrum for $E(B-V) = 0.2$ increases the temperature of the single WD model by 3000 K and reduces the distance by a factor of 2. The χ^2 obtained is slightly lower $\chi^2_\nu \approx 0.096$. For the single disk models, the mass accretion rate obtained is larger by a factor of up to ∼30, while the distance is reduced by about half (all the models are listed in Table 4). Again, there is not much difference between the single disk model and the single WD model. The WD+disk composite models again do not bring any improvement in the fit, rather the opposite.

It is most likely that the spectrum is solely due to the heated WD as the system was observed in a relatively low state. The best disk models reach a mass accretion rate that is very large for such a low state. Our preferred model is the single WD model for $E(B-V) = 0.2$, assuming an intermediate mass of $0.8\,M_\odot$ with $T = 43{,}000$ K. This model is shown in Figure 2.

4.1.2. AQ Mensae/EC 05114-7955

AQ Men (also known as EC 05114-7955 (Cheng et al. 2001)) has a magnitude around 14–15, but no outburst has been detected so far. Its period is 0.141466 days (Patterson 2002). Its optical spectrum suggests that it is a DN; however, the possibility that it is an NL cannot be ruled out (Cheng et al. 2001). Cheng et al. (2001) classified it as an *unusual/peculiar* CV that shows large-amplitude flickering and a low-excitation spectrum, where the C III/N III λ 4650 Å blend is also seen in emission and suggested that the double peak in the line profiles might indicate that it is a highly inclined system. Patterson (2002) showed that it is actually an eclipsing system with superhumps and a precession period of 3.77 ± 0.05 days.

A *FUSE* spectrum of AQ Men was obtained on 2006 November 22, at which time we only knew it was at a magnitude between 14 and 15 (AAVSO data). For the modeling, we do not know a priori whether the disk or the WD dominates the FUV spectrum. In spite of its very low continuum flux level (at most $\sim 1 \times 10^{-14}$ erg cm^{-2} s^{-1} Å^{-1}; see Figure 3), the spectrum (binned at 0.2 Å) exhibits features that are easily identified such as the molecular hydrogen absorption lines, some Si III and Si IV, and C III absorption features, as well as broad emission from the O VI doublet and the C III (1175) multiplet. The emission is consistent with DNs observed in quiescence, and

Table 4
Synthetic Spectra

System Name	M_{wd} ($M_\odot$)	T_{wd} (10^3 K)	$V_{\rm rot}\sin i$ (km s^{-1})	i (deg)	Log($\dot{M}$) ($M_\odot$ yr^{-1})	WD/Disk (%)	d (pc)	χ^2_ν	E_{B-V}	Figure
HP Nor	0.4	34	1000	···	···	WD	1134	0.105	0.00	
	0.8	37	1000	···	···	WD	648	0.107	0.00	
	1.2	40	1000	···	···	WD	381	0.105	0.00	
	0.55	···	···	60	−8.5	Disk	1448	0.105	0.00	
	0.8	···	···	<4	−9.0	Disk	1603	0.104	0.00	
	1.2	···	···	8	−10.0	Disk	1021	0.101	0.00	
	0.4	40	1000	···	···	WD	530	0.096	0.20	
	0.8	43	1000	···	···	WD	265	0.096	0.20	2
	1.2	46	1000	···	···	WD	148	0.096	0.20	
	0.55	···	···	18	−8.0	Disk	1060	0.097	0.20	
	0.8	···	···	18	−8.0	Disk	1800	0.093	0.20	
	1.2	···	···	18	−8.5	Disk	1515	0.095	0.20	
AQ Men	0.4	24	···	···	···	WD	710	···	0.00	
	1.1	36	···	···	···	WD	710	···	0.00	
	0.35	···	···	81	−8.75	Disk	710	···	0.00	
	1.20	···	···	81	−9.5	Disk	710	···	0.00	
	0.4	28.5	···	···	···	WD	710	···	0.10	
	1.1	60	···	···	···	WD	710	···	0.10	
	0.35	···	···	81	−7.9	Disk	710	···	0.10	
	1.20	···	···	81	−8.9	Disk	710	···	0.10	
V433 Ara	0.4	···	···	81	−8.5	Disk	1200	···	0.00	
	0.4	···	···	81	−8.0	Disk	1200	···	0.10	
	1.2	···	···	81	−9.5	Disk	1200	···	0.00	
	1.2	···	···	81	−9.0	Disk	1200	···	0.10	
	0.4	24	···	···	···	WD	1200	···	0.00	
	0.4	28	···	···	···	WD	1200	···	0.10	
	0.8	30	···	···	···	WD	1200	···	0.00	
	0.8	40	···	···	···	WD	1200	···	0.10	
	1.2	40	···	···	···	WD	1200	···	0.00	
	1.2	75	···	···	···	WD	1200	···	0.10	
DT Aps	⩽1.2	···	···	18	⩾ −10	Disk	⩾2800	0.213	0.00	
	⩽1.2	···	···	18	⩾ −9.5	Disk	⩾2950	0.223	0.09	
	⩾0.4	⩾34	500	···	···	WD	⩾1000	0.212	0.00	
	0.8	37	500	···	···	WD	1700	0.205	0.00	6
	⩾0.4	⩾36	500	···	···	WD	⩾625	0.225	0.09	
NSV 10934	0.8	···	···	75	−10	Disk	185	0.196	0.00	
	1.2	···	···	81	−10.5	Disk	144	0.160	0.00	
	0.4	···	···	75	−9	Disk	179	0.202	0.10	
	0.8	···	···	80	−9.5	Disk	157	0.172	0.10	
	1.2	···	···	81	−10	Disk	187	0.146	0.10	8
	1.2	30	···	···	···	WD	216	0.232	0.10	
AM Cas	⩽0.8	···	···	⩽60	⩾ −9.5	Disk	350	0.611	0.00	
	0.40	30	1000	···	···	WD	307	0.623	0.00	
	0.80	36	500	18	−9.7	41/59	373	0.563	0.00	10
	0.55	35	400	18	−8.5	11/89	331	0.538	0.20	11
FO Per	0.40	···	···	75	−8.5	Disk	251	0.296	0.00	
	0.80	···	···	60	−9.5	Disk	295	0.313	0.00	
	⩾0.40	⩾25	400	···	···	WD	266	⩾0.312	0.00	
	0.40	21	200	75	−8.5	29/71	291	0.258	0.00	13
	1.00	···	···	18	−9.0	Disk	281	0.172	0.30	
	⩾0.40	35	200	···	···	WD	⩽135	0.152	0.30	
	⩾0.40	40	200	18	⩽ −8.5	52/48	⩽254	0.146	0.30	14
ES Dra	1.20	···	···	5	−9.5	Disk	770	0.4280	0.00	16
	0.58	35	700	···	···	WD	770	0.4277	0.00	17

the large (rotational) broadening of the C III emission (>6 Å, or $v > 1000$ km s^{-1}) agrees with the fact that it is highly inclined. However, broad emission lines are also often observed in nova-like systems. In the present case, the *FUSE* spectrum of AQ Men is more similar to that of a quiescent DN such as EK TrA (Godon et al. 2008a), as the emission lines are not as strong as those exhibited by nova-like systems (such as AE Aqr; see the *MAST* archive).

The distance to AQ Men (using the relations of Warner 1987; Harrison et al. 2004; see Table 3) is possibly $d \approx 710$ pc. AQ Men has no known reddening but the Galactic reddening in its direction is $E(B-V) = 0.18$. We model its *FUSE* spectrum first assuming no reddening, and then assuming $E(B-V) = 0.10$. Since it is apparently an eclipsing system (Patterson 2002), we set the inclination angle to $i = 81^\circ$. The spectrum of AQ Men is so poor that we only try to fit the flux level in order to obtain the

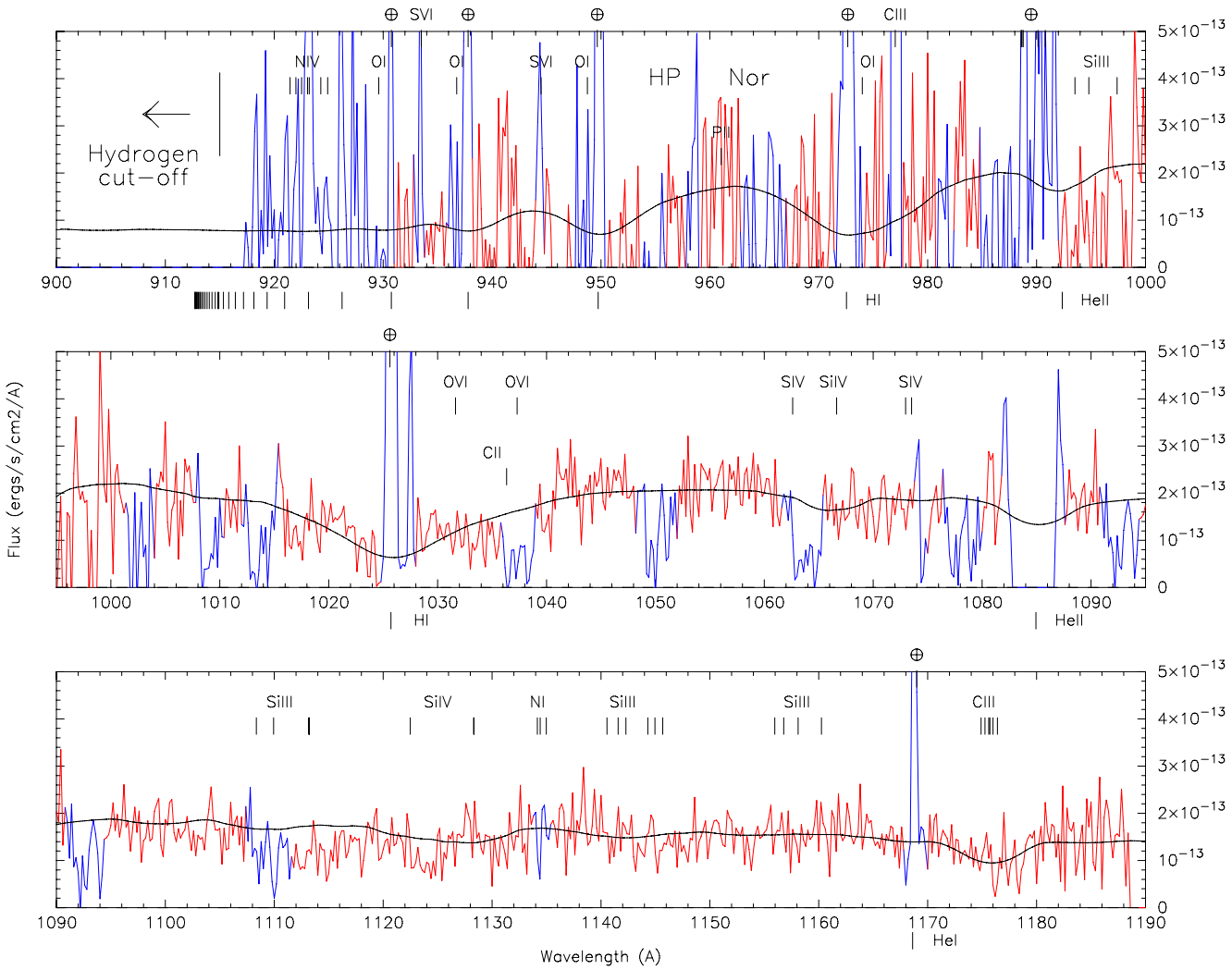

Figure 2. Best-fit model to the *FUSE* spectrum of HP Nor assuming $E(B-V) = 0.2$. The model is in black, the observed spectrum is in red (light gray), and the regions that have been masked before the fitting are in blue (dark gray). The model consists of a WD with $M = 0.8\,M_{\odot}$, $T = 43{,}000$ K, and a projected rotational velocity $v_{\rm rot} \sin i = 1000$ km s^{-1}. The distance obtained is $d = 265$ pc.

(A color version of this figure is available in the online journal.)

distance to the system irrelevant of the value of the χ^2. Since we only fit the flux level, we do not show any figure of the results.

Single Disk Model. For the single disk model fit, we find that in order to fit the distance, the mass accretion rate has to be $\dot{M} = 10^{-9.5}\,M_{\odot}$ yr^{-1} assuming a WD mass of $1.2\,M_{\odot}$; and it increases to $\dot{M} = 10^{-8.75}\,M_{\odot}$ yr^{-1} for $M_{wd} = 0.35\,M_{\odot}$. Next, we carried out the same model fits, but we deredden the spectrum assuming $E(B-V) = 0.1$. We obtain larger mass accretion rates as listed in Table 4. From these single disk models, we note that if the emission is due to a disk, then its accretion rate is consistent with the outburst state of a DN, where the minimum value obtained ($\dot{M} = 10^{-9.5}\,M_{\odot}$ yr^{-1}) is for the larger mass ($1.2\,M_{\odot}$) assuming no reddening. This is the lower limit of $\dot{M}$ for all reasonable values of M_{wd} ($\leqslant 1.2\,M_{\odot}$) and $E(B-V) \geqslant 0.0$.

Single WD Model. Assuming no reddening and for a mass $M = 0.4\,M_{wd}$, we fit the flux with $T = 24{,}000$ K. Increasing the mass decreases the radius and therefore the flux is fit with a larger temperature reaching 36,000 K for a $1.1\,M_{\odot}$ WD. Dereddening the spectrum assuming $E(B-V) = 0.10$, we obtain higher temperatures, with $T = 60{,}000$ K for $M = 1.1\,M_{\odot}$. From the single WD modeling, we obtain that if the spectrum is due to the WD alone, then its temperature must be $T \geqslant 24{,}000$ K and it increases with increasing mass and reddening. This is, therefore, the lower limit for the WD temperature of AQ Men, assuming its spectrum is solely from the WD. Since there is no additional constraints on the parameters of the system, we are unable to carry out a multicomponent (WD+Disk) model fit as there is degeneracy. However, we note that because of its inclination (Patterson 2002), the disk masks the WD, except if it is in a quiescent-like state.

For AQ Men, we can summarize these results as follows. If the system is a DN, then it is probably in a lower state, where the WD dominates the FUV and has a temperature of at least 24,000 K. The disk models do not agree with a quiescent mass accretion rate for DN. If the system is an NL, then the disk is in outburst and dominates the FUV with a mass accretion rate $\dot{M} \leqslant 3 \times 10^{-10}\,M_{\odot}$ yr^{-1}, barely larger than $\dot{M}_{\rm critic}$ but consistent with the theory.

4.1.3. V433 Arae/S 6006

V433 Ara is an eclipsing Z Cam DN system, with a period of 4.698 hr (Woudt et al. 2005). From the AAVSO data, we find that the system was in quiescence at the time of the *FUSE* observations, on 2007 February 18. However, its exact magnitude during the *FUSE* observations is not known. The

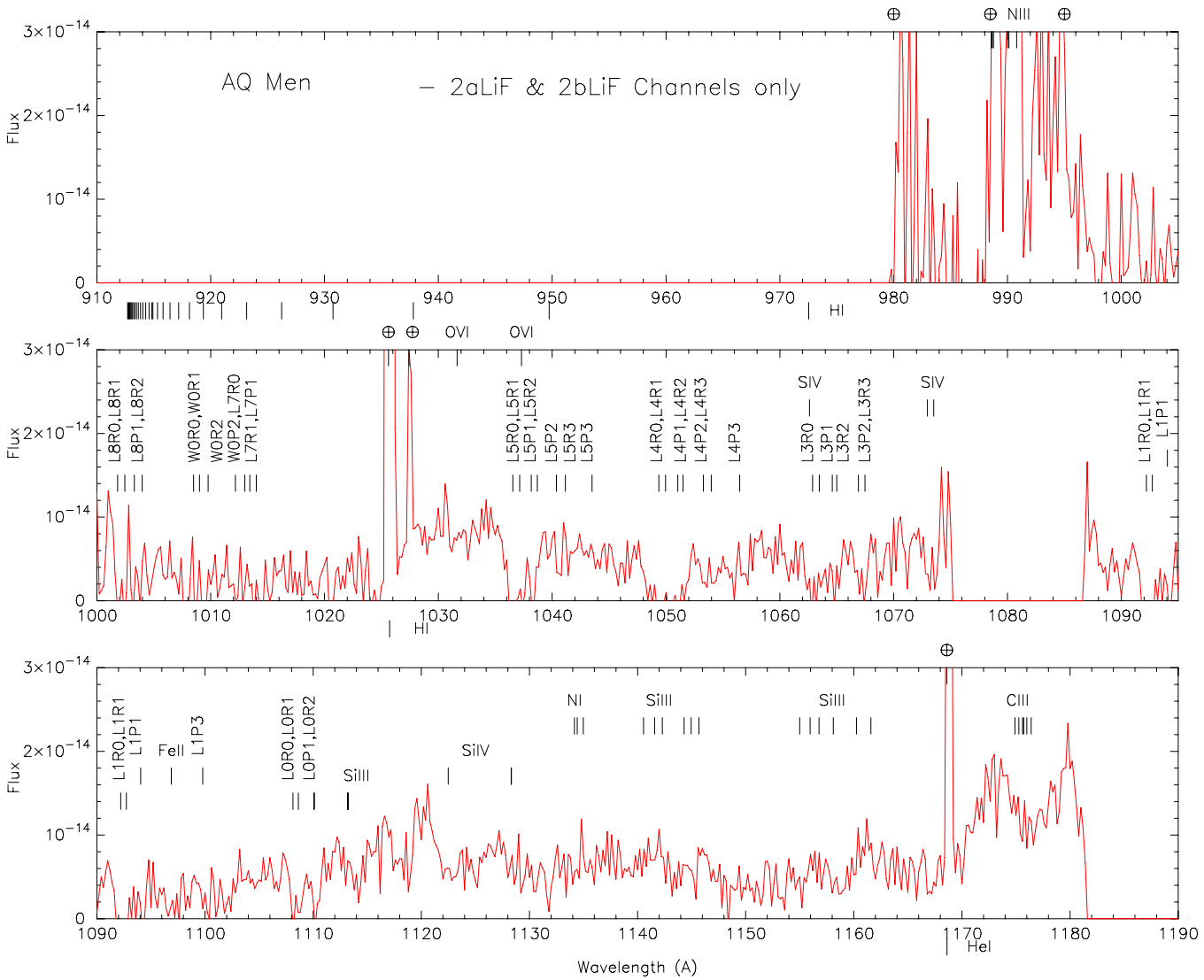

Figure 3. *FUSE* spectrum of AQ Men. Due to their contamination with airglow and very low signal, the LiF 1 and SiC 1 and 2 channels have been discarded. Even though the signal is very poor, one recognizes the ISM molecular absorption features (labeled vertically), as well as some broad emission from C III (1175) and the O VI doublet. One can identify the Si III (1113 Å) and Si IV (1123 and 1128 Å) lines. Other metal lines have been marked but are not detected.

(A color version of this figure is available in the online journal.)

FUSE spectrum of V433 Ara (Figure 4) is the poorest spectrum of all the observed spectra we model; it consists only of the LiF channels and, consequently, we are not able to model it properly. We model only the flux level to obtain some constraints on the temperature and mass of the WD and possibly on the mass accretion rate. The Galactic reddening in the direction of V433 Ara is about 0.2 but the actual reddening of V433 Ara is not known. We assume here $E(B-V) = 0.0$ and 0.1. Also from the period–luminosity relation, we find a distance of ∼1200 pc. Since the system was not observed in outburst, the spectrum could be that of either quiescence (∼18 mag) with the WD dominating the spectrum, or standstill (∼16.5 mag) at an intermediate level (Woudt et al. 2005) where the inflated disk dominates the spectrum (because of the high inclination). We model the spectrum with single disk and single WD models, fixing $d = 1200$ pc and $i \sim 80°$. Since the spectrum is of such a poor quality (see Figure 4), we do not show the model, as we only fit the *level of the continuum* (i.e., there are no features to match).

Single Disk Models. The main results for the disk model are presented in Table 4. For a larger WD mass, the mass accretion needed to fit the spectrum decreases. If the system was observed with *FUSE* in a standstill, then the mass accretion rate should rather be on the lower side in agreement with a large WD mass and little reddening. However, because of the large distance, the reddening might not be negligible and we therefore suspect that V433 Ara could have been observed in quiescence and that its FUV flux might be due to a WD rather than a disk.

Single WD Models. The WD models are listed in Table 4. The main result is that the temperature of the WD increases with the mass of the WD and the reddening. From these, it appears that the lower limit for the WD temperature of V433 Ara is 24,000 K. Again, if the reddening is not negligible ($E(B-V) = 0.1$ or larger), then the WD mass has an upper limit of about 0.8–1.0 $M_\odot$, as it is very unlikely that the WD has a temperature $T \sim 75{,}000$ K (most DNs' WDs have $T < 50{,}000$ K).

4.1.4. DT Apodis/S 5646

DT Aps was first identified as a DN by Vogt & Bateson (1982), and it is classified as an SS Cyg subtype (Downes

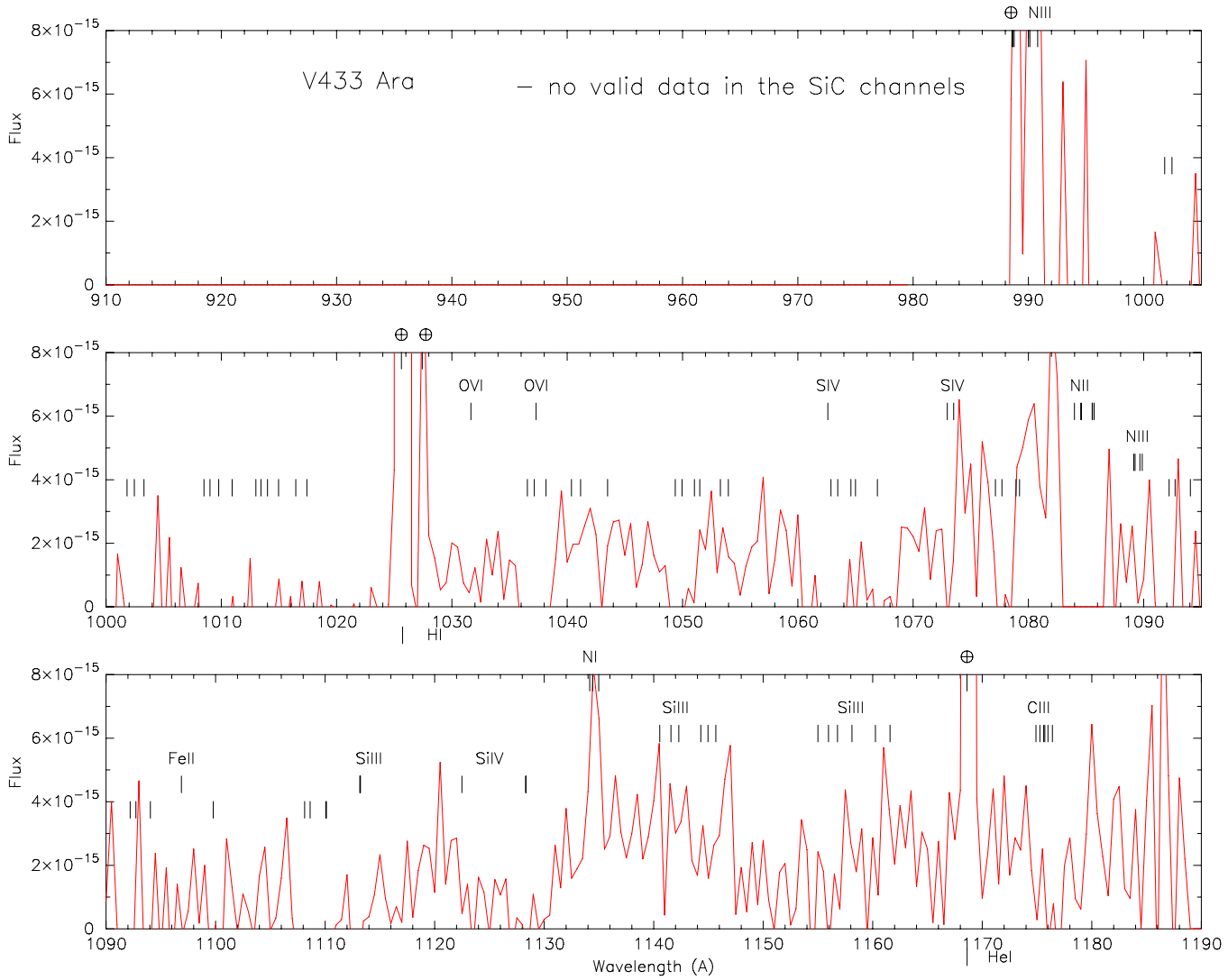

Figure 4. *FUSE* spectrum of V433 Ara. Due to their contamination with airglow and very low signal, the SiC 1 and 2 channels have been discarded. The S/N is so poor that it is impossible to model any features, instead the flux level is used to assess a limit on the WD temperature and/or the disk mass accretion rate. We have marked the ISM molecular lines as well as the metals lines usually seen in spectra of quiescent DNs. Some lines coincide (e.g., C III 1175 Å) with a dip in the flux, but no lines are actually detected as the flux also dips in region where lines are not expected to be observed (e.g., 1150 Å).

(A color version of this figure is available in the online journal.)

et al. 2001). Apart from that, little is known about this high-declination southern dwarf nova.

DT Aps was observed with *FUSE* on 2006 April 28 and on 2006 May 3. These observations were taken four and nine days (respectively) after an outburst was recorded by the AAVSO on 2006 April 24. It is not known how long the outburst lasted, but it is likely that the first observation caught the system while it was still in a relatively active state. The second observation was taken after the system had more time to decline to quiescence; however, it was 10 times shorter than the first one and it is therefore unusable. Even though the first observation lasted basically 70 ks, the SiC channels were very noisy and large portions of the spectral segments had to be discarded. The *FUSE* spectrum of DT Aps is shown in Figure 5.

In the shorter wavelengths (the upper panel), the spectrum consists mainly of sharp airglow emission lines (noise) with some possible C III (λ977) emission; at longer wavelengths (the middle panel) the spectrum reveals a prominent broad and deep Lyβ absorption feature, which is the main feature of the spectrum. In the longer wavelengths (the lower panel), the silicon absorption features Si III and Si IV (around $\lambda \sim 1110$–1130 Å) are very deep and could possibly indicate a high silicon abundance. However, since the other silicon absorption features are not as pronounced, it is likely that the deep silicon features are due to incorrect background subtraction. Alternatively, there could be some emitting components contributing some flux around $\lambda \sim 1150$–1160 Å. The C III (λ1175) absorption multiplet is also rather deep and broad, possibly due to a large velocity broadening. The spectrum is rather noisy and of poor quality, making it difficult to model.

Since the period of the system is not known, we have no way to estimate its distance. The reddening of the source is also not known, but the Galactic reddening in its direction is $E(B-V) = 0.09$. A reddening of 0.05 will not affect the results by much and, therefore, in order to assess the effect of the reddening on the results, we carry out model fits assuming both $E(B-V) = 0.0$ and $E(B-V) = 0.09$. Since the system was observed four days after an outburst, the flux is due to either a disk (with a lower accretion rate than the peak outburst) or a heated WD, or both.

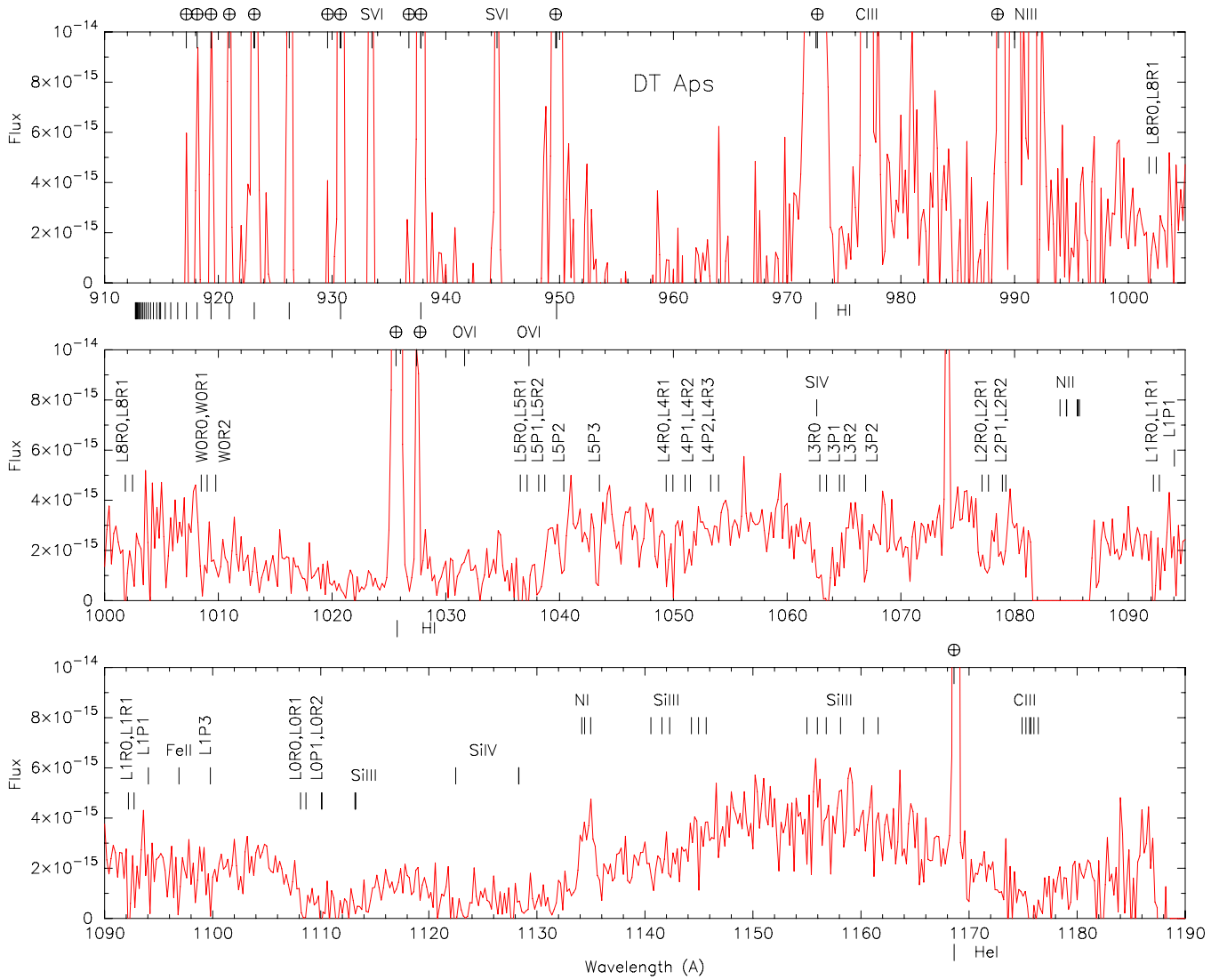

Figure 5. *FUSE* spectrum of DT Aps. In the upper panel the spectrum consists mainly of sharp airglow emission lines; at longer wavelengths, in the middle panel, the spectrum reveals a prominent broad and deep Lyβ absorption feature. In the longer wavelengths (the lower panel) the silicon absorption features Si III and Si IV (around $\lambda \sim 1110$–1130 Å) are very deep and there seems to be some emission around $\lambda \sim 1150$–1160 Å , and both could be due to an incorrect background subtraction. The broad C III (λ1175) absorption feature is the sign of a large velocity broadening. The only lines that are identified are the ISM molecular lines and the C III (1175 Å) line, and all the other lines have been marked but not detected. Overall, the spectrum is rather noisy and of a poor quality.

(A color version of this figure is available in the online journal.)

Single Disk Models. For a $0.35\,M_{\odot}$ WD, the best disk model has $\dot{M} = 10^{-8.5}\,M_{\odot}$ yr^{-1}, $i = 18^{\circ}$, $d = 4450$ pc, and $\chi^2 = 0.2127$. As we increase the WD mass, the mass accretion rate needed to fit the spectrum decreases and for a $1.2\,M_{\odot}$ WD, the best disk model has $\dot{M} = 10^{-10}\,M_{\odot}$ yr^{-1}, $i = 18^{\circ}$, $d = 2800$ pc, and $\chi^2 = 0.2138$. The difference in the χ^2 value between these best-fit models is not significant and we have therefore no way to find out the mass of the WD from these fits. We note that since the system was observed *after* an outburst, it is clear that its mass accretion rate is much lower than at outburst, consistent with the higher WD mass and smaller distance. Next, we deredden the spectrum assuming $E(B-V) = 0.09$ and carry out the same procedure (since the distance we obtained is very large, it is likely that the spectrum is affected by reddening). We find a slightly larger mass accretion rate (with about the same distance) and a χ^2 value larger by about 5%–10%. The smaller mass accretion rate is obtained for the $1.2\,M_{\odot}$ WD, with $\dot{M} = 10^{-9.5}\,M_{\odot}$ yr^{-1}, $i = 18^{\circ}$, $d = 2950$ pc, and $\chi^2 = 0.2273$. None of the disk models provided an adequate fit to the spectrum as the deep and broad absorption feature around 1130 Å and the "hump" feature around 1160 Å could not be fit.

Single WD Models. The lowest mass model ($M = 0.4\,M_{\odot}$) gives a temperature of 34,000 K, a distance of ~3000 pc, and $\chi^2 = 0.2115$; while the largest mass model ($M = 1.2\,M_{\odot}$) gives a temperature of 40,000 K, a distance of ~1000 pc, and $\chi^2 = 0.2125$. These models do not provide a better fit than the single disk models. We then ran an intermediate mass model ($M = 0.8\,M_{\odot}$) with an increased silicon abundance and found that the fit could be slightly improved when Si > 10 × solar. That best-fit model has $T = 37{,}000$ K, $d = 1700$ pc, and $\chi^2 = 0.2050$ (see Figure 6). In order to fit the C III (λ1175) line profile, all these models have a rotational velocity of about 500 km s^{-1}. Here too we check how a reddening of $E(B-V) = 0.09$ affects the results and we find no improvement, rather the opposite, the χ^2 is larger by about

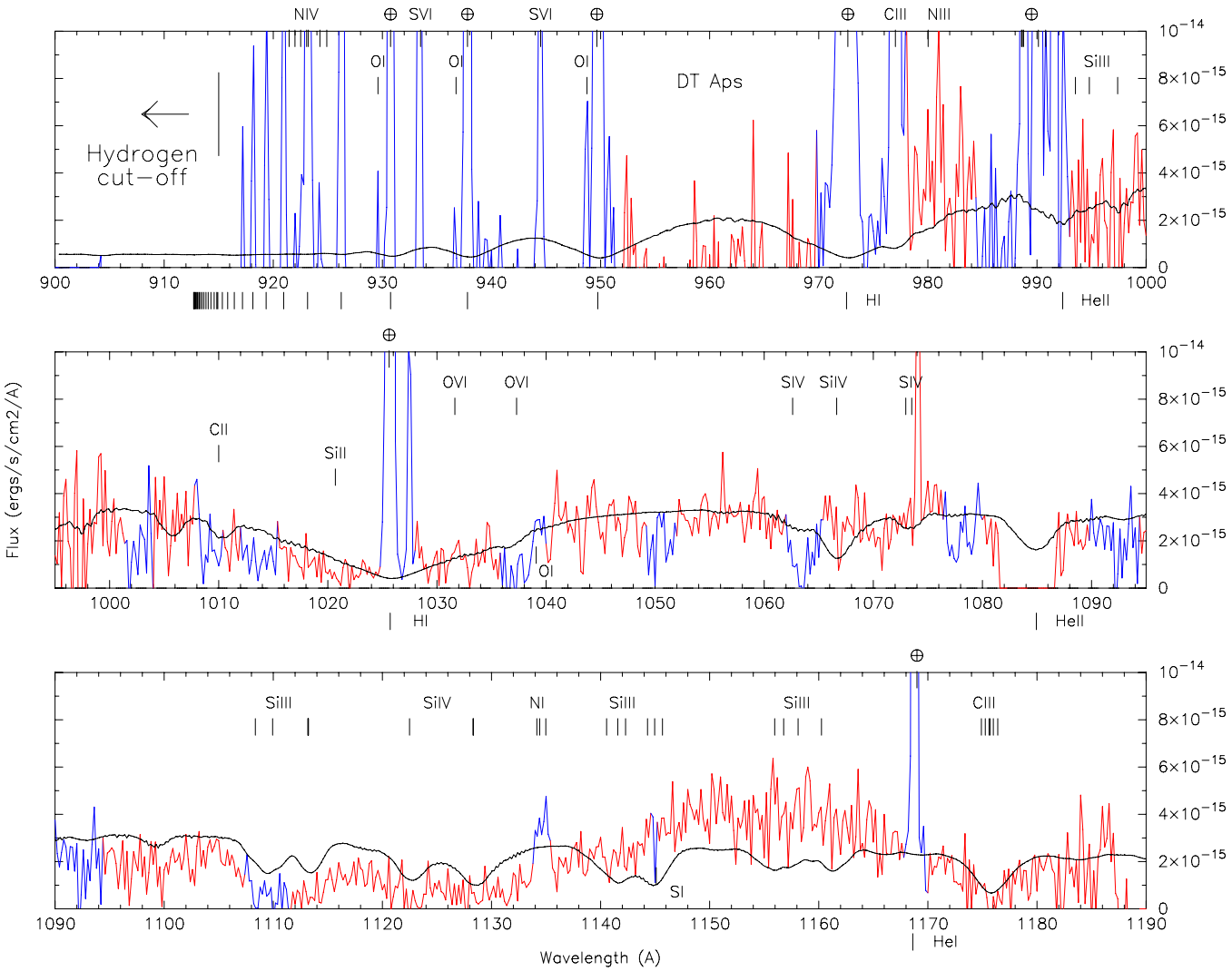

Figure 6. Best-fit model (in black) to the *FUSE* spectrum (in red/light gray) of DT Aps. The regions that have been masked before fitting are in blue/dark gray (they consist mainly of ISM molecular hydrogen absorption lines and airglow emission). The model consists of a WD with a mass $M = 0.8\,M_{\odot}$, with $T = 37{,}000$ K, a silicon abundance of 10× solar, $d = 1700$ pc, and $\chi^2 = 0.2050$. In order to fit the absorption line profiles, the projected rotational velocity $V_{\rm rot} \sin i$ was set to 500 km s^{-1}. Here we assumed $E(B-V) = 0.0$.

(A color version of this figure is available in the online journal.)

5%–10%. The smallest distance is obtained for the $M = 1.2\,M_{\odot}$ model, with $T \sim 42{,}000$ K, $d = 624$ pc, and $\chi^2 = 0.2290$.

Lastly, we tried composite WD+disk models, but they did not improve the fit, and because of the unknown mass, distance, and inclination, the results for the composite models were inconclusive.

4.1.5. NSV 10934/Oct

NSV10934 is a SU UMa subtype dwarf nova (Kato et al. 2002, 2004; Downes et al. 2001). It shows superoutbursts (Kato et al. 2004) during which superhumps are detected with a period of 0.07478 days. Shorter (normal) outbursts occur at intervals of about 40–60 days. However, due to the unusual rapid fading of its normal outbursts, Kato et al. (2004) note that it may be an intermediate polar (IP) candidate showing SU UMa properties.

NSV 10934 was observed with *FUSE* on 2006 June 28 (JD2453914.6), and on 2006 June 30 (JD2453916.7), 28 days (or possibly less) after the end of an outburst lasting a week. At the time of the *FUSE* observation, the system was in quiescence. The *FUSE* spectrum of NSV 10934 consists of five orbits from the first data set and four orbits from the second data set combined together (Figure 7). The system was possibly at a magnitude of ∼15.5–16.0. The flux level of the spectrum is very low and the *FUSE* spectrum suffers from a very low S/N. In spite of that, we see that there is a rather flat continuum with very broad emission lines from C III (λ977 and λ1175) and the O VI doublet. The broad emission lines are an indication that the system is viewed at a high-inclination angle, possibly $i \geqslant 60^{\circ}$ (see, e.g., the broad emission lines of the DN EK TrA, with $i = 60^{\circ}$, in quiescence; Godon et al. 2008a). Since eclipses have not been detected, we can assume $i < 80^{\circ}$. The Lyβ broad absorption feature is not detected, possibly due to the left wing of the very broad oxygen emission feature. However, in that respect, the continuum is a priori more characteristic of an accretion disk seen at a high-inclination angle. Therefore, in the following, we model the *FUSE* spectrum of NSV 10934 with a single WD, a single disk, and a WD+disk. We also assume two reddening values, $E(B-V) = 0$ and $E(B-V) = 0.1$ to assess how reddening affects the results. Using the period–luminosity relation, we find that the distance to the system is possibly $d \sim$ 150 pc (see Table 3).

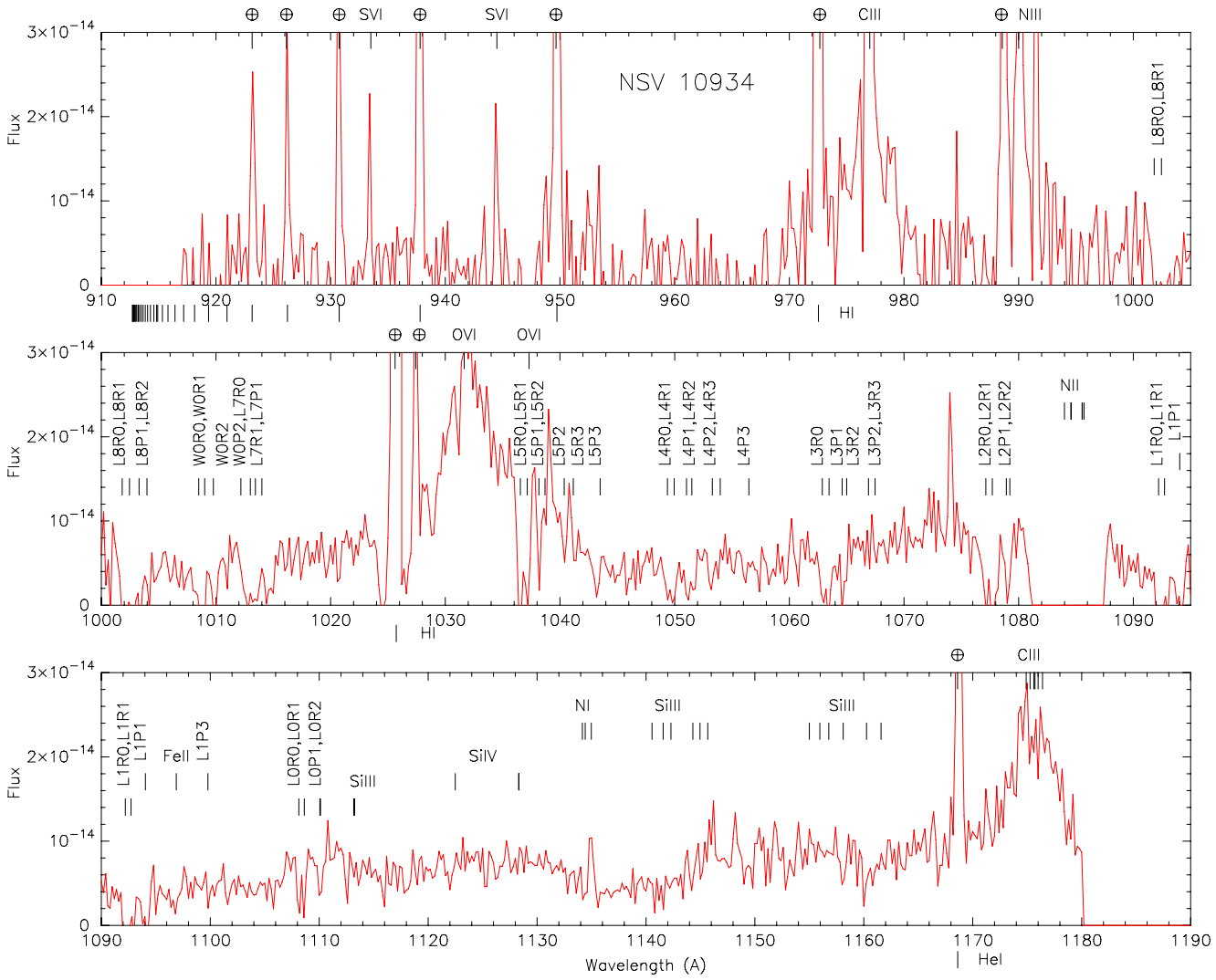

Figure 7. *FUSE* spectrum of NSV 10934 has a low S/N especially in the shorter wavelengths due to the fact that the data from the 2bSiC, 2bLiF, and 1aSiC channels were unusable and a large portion of the 1bLiF channel was lost to the worm. As a consequence, there is a gap around 1085 Å. The continuum is rather flat with very broad emission lines from C III (λ977 and λ1175) and the O VI doublet. The Lyβ broad absorption feature is not detected, possibly either due to the left wing of the very broad oxygen emission feature or due to velocity broadening in a disk viewed at a high inclination. The ISM molecular lines are identified (labeled vertically). The metal lines have been marked but are not detected. All the sharp emission lines are due to airglow.

(A color version of this figure is available in the online journal.)

WD models. Since NSV 10934 was observed in quiescence and has been classified as a DN, we decided to model its *FUSE* spectrum first with a single WD. For any WD mass between 0.4 and 1.2 $M_{\odot}$, there is no synthetic spectrum that can fit the observed spectrum and the distance at the same time. In order to fit the flux between 1000 Å and 1080 Å, the temperature of the WD has to be of the order of 25,000 K and higher (depending on the mass) and this leads to a distance well above 200 pc. The WD models that lead to a distance of about 200 pc have a lower temperature and do not fit the continuum of the spectrum at all. We then decided to deredden the observed spectrum assuming $E(B-V) = 0.1$ to see if this improves the modeling and the best model obtained in this case is for a 1.2 $M_{\odot}$ WD with a temperature of 30,000 K. This WD model gives a distance of 216 pc and $\chi^2 = 0.232$, and it is barely better than the WD models obtained without dereddening the spectrum. We remark here that the worst models obtained are for the lower WD masses.

Disk Models. Since the WD models are less than satisfactory, we decided to run single disk models, first assuming $E(B-V) = 0.0$. For $M_{wd} = 0.4\,M_{\odot}$, the mass accretion rate needed to fit the spectrum is very large for quiescence and gives a distance far too large. For $M_{wd} = 0.8\,M_{\odot}$, the best-fit model has $\dot{M} = 10^{-10}\,M_{\odot}$ yr^{-1} and $i = 75^{\circ}$, and gives a distance of 185 pc and $\chi^2 = 0.196$. The best-fit model, however, is obtained for the largest mass in the run with $M_{wd} = 1.2\,M_{\odot}$, $\dot{M} = 10^{-10.5}\,M_{\odot}$ yr^{-1}, and $i = 81^{\circ}$, and gives a distance of 144 pc and $\chi^2 = 0.160$ (all shown in Table 4). Next, we dereddened the spectrum assuming $E(B-V) = 0.1$, the best-fit model is for $M_{wd} = 1.2\,M_{\odot}$ with $\dot{M} = 10^{-10}\,M_{\odot}$ yr^{-1} and $i = 81^{\circ}$, which gives a distance of 187 pc and $\chi^2 = 0.146$. This best-fit model is shown in Figure 8. All the models are listed in Table 4.

At this stage, we tried to add a WD spectral component to the synthetic disk spectrum, but it did not improve the fit. We note that with this inclination the WD might not be visible even with a low-mass accretion rate, as the outer part of the disk might be masking it. The high inclination is also in agreement with the large broadening of the carbon and oxygen emission features.

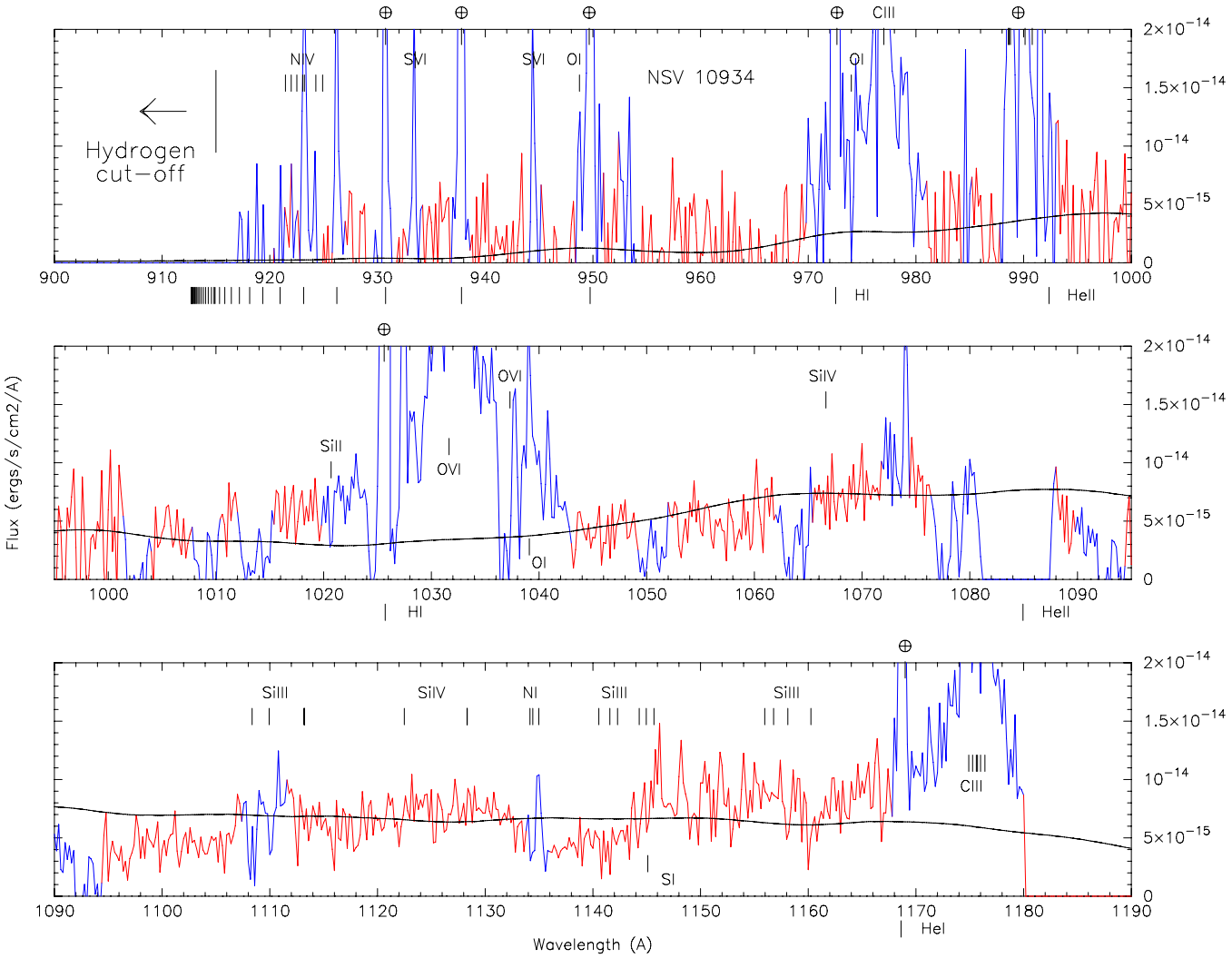

Figure 8. Best-fit model to the *FUSE* spectrum of NSV 10934. The observed spectrum (in red/light gray) has been dereddened assuming $E(B-V) = 0.1$. The regions that have been masked before modeling are shown in blue (dark gray). The best fit (in black) consists of a disk model with an $M = 1.2\,M_{wd}$, $\dot{M} = 10^{-10}$, and $i = 81^{\circ}$, giving a distance of 187 pc $\chi^2 = 0.146$.

(A color version of this figure is available in the online journal.)

4.2. Northern Hemisphere Systems

4.2.1. AM Cassiopeiae/258.1928

Because of its short-period activity and relatively high brightness (12.3–15.2 mag; Downes et al. 2001), AM Cas was discovered long ago by Hoffmeister (1929). Its relation to dwarf novae was suggested by Richter (1961), who observed a nine days outburst cycle and the occurrence of standstills. It was classified as a Z Camelopardalis system by Notni & Richter (1984). Optical spectra were later obtained by Richter et al. (1988), who confirmed the classification of AM Cas as a Z Cam DN as well as its short (mean) outburst cycle period (8.2 days). The orbital period of the binary system is 0.165 days (= 3.96 hr) as reported by Taylor & Thorstensen (1996), who also obtained three optical spectra ∼4500–6300 Å. One of the spectra is in quiescence with a flux $< 10^{-15}$ erg s^{-1} cm^{-2} Å^{-1}, and the two other spectra are in an intermediate state with a maximum flux reaching $\sim 10^{-14}$ erg s^{-1} cm^{-2} Å^{-1} at 4500 Å and decreasing toward longer wavelengths.

AM Cas was observed with *FUSE* on 2006 October 19 (JD 2454027.1) and the AAVSO data indicated that it was in standstill at that time with a visual magnitude of 13.8 (the system can reach 12.3 mag). The *FUSE* spectrum has a continuum flux level reaching 1.5×10^{-13} erg s^{-1} cm^{-2} Å^{-1} (Figure 9), which makes AM Cas the brightest FUV target we observed.

The *FUSE* data for AM Cas consist of six exposures (i.e., orbits). The quality of the spectrum is relatively good and reveals some moderate ISM molecular hydrogen absorption lines. The C III (1175) line might be blueshifted by 3 Å; however, this is the region affected by the worm and the feature might be an artifact of the worm rather than a true absorption feature. In the short wavelengths (<950 Å), the flux does not reach zero and the continuum there is about 1/3 of the flux at longer wavelengths (>1000 Å), indicative of a high temperature. On the other hand, the Lyβ is rather deep and wide, indicative of a lower temperature. It is possible that the flux in the shorter wavelengths is due to broad emission lines from N IV (∼ λ923), S VI (λλ935, 945), similar to the broad feature around 976 Å–980 Å due to C III (λ977) and N III (λ980). However, there is no sign of emission from the O VI doublet. Another possibility is that of two emitting components (disk+WD), one is contributing relatively more flux in the shorter wavelengths, and the other having a deep Lyβ profile. Since we know that AM Cas was

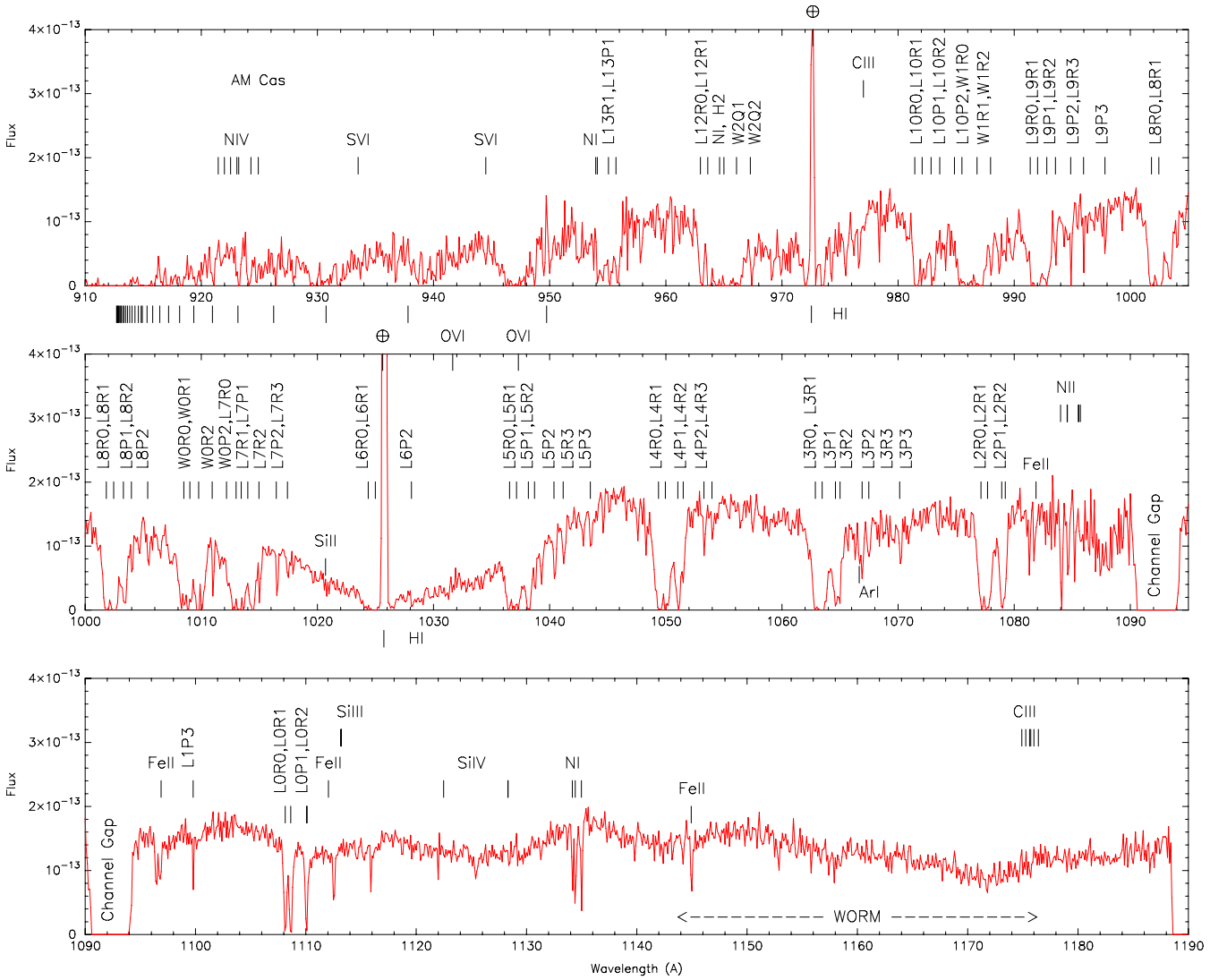

Figure 9. *FUSE* spectrum of AM Cas with line identifications. The ISM molecular hydrogen absorption lines have been labeled vertically. This spectrum consists only of the 1-SiC and -LiF a and b channels, because of that there is a gap around 1095 Å, and the longer wavelengths are affected by the worm (as shown). The higher ionization level metal lines are discussed in Figure 11 in the context of the fit model.

(A color version of this figure is available in the online journal.)

observed in an intermediate (standstill) state, we may expect that both the WD and the disk contribute to the flux. For the modeling, we assess a distance of 350 pc using the period–luminosity relation (see Table 3). The reddening of AM Cas is not known; however, the Galactic reddening in its direction is pretty large (∼0.9) and it is therefore possible that AM Cas itself has a significant reddening. For this reason, we model the *FUSE* spectrum of AM Cas, assuming no reddening and assuming a reddening of 0.2, as this allows us to assess how the reddening affects the results. We first ran models assuming $E(B-V) = 0.0$.

Single Disk Models. The single disk models are unable to fit the deep Lyβ feature and the flux in the shorter wavelengths at the same time. The best models (least χ^2, and consistent with the distance and outburst state) are as follows. For a WD mass $M_{wd} = 0.4\,M_\odot$, $\dot{M} = 10^{-8.5}\,M_\odot$ yr^{-1}, $i \approx 60°$, $d = 324$ pc, and $\chi^2 = 0.611$; as the mass increases to $M_{wd} = 0.8\,M_\odot$, we get $\dot{M} = 10^{-9.5}\,M_\odot$ yr^{-1}, $i \approx 20°$, $d = 376$ pc, and $\chi^2 = 0.614$. From the single disk models alone, we infer that the mass of the WD must be $M_{wd} \leqslant 0.8\,M_\odot$, the system must have an inclination $i \leqslant 60°$ and the mass accretion rate in outburst is $\dot{M} = 10^{-9.5}$ to $10^{-8.5}\,M_\odot$ yr^{-1}.

Single WD Models. The best-fit model was obtained for a $0.4\,M_\odot$ WD with a temperature of 30,000 K, a projected rotational velocity of 1000 km s^{-1}, a distance of 307 pc, and $\chi^2 = 0.623$. Models with a larger mass (and consequently a smaller radius) gave an even smaller distance. The single WD model indicates, as the single disk model, a rather small mass and an intermediate temperature.

Composite WD+Disk Models. For the composite WD plus disk models, we initially chose an average WD mass of $0.8\,M_\odot$. We find that the least χ^2 model is for a mass accretion of $2 \times 10^{-10}\,M_\odot$ yr^{-1}, an inclination $i = 18°$, a WD temperature $T = 36{,}000$ K with a projected rotational velocity $V_{\rm rot} \sin i = 500$ km s^{-1}. This gives a distance of 373 pc, $\chi^2 = 0.563$, with the WD contributing 41% of the flux and the disk 59%. This model, though better than the single WD and single disk models, also does not fit well the high flux in the lower wavelengths. This model is shown in Figure 10. In order to fit the lower wavelength region of the spectrum, we have to increase the temperature of

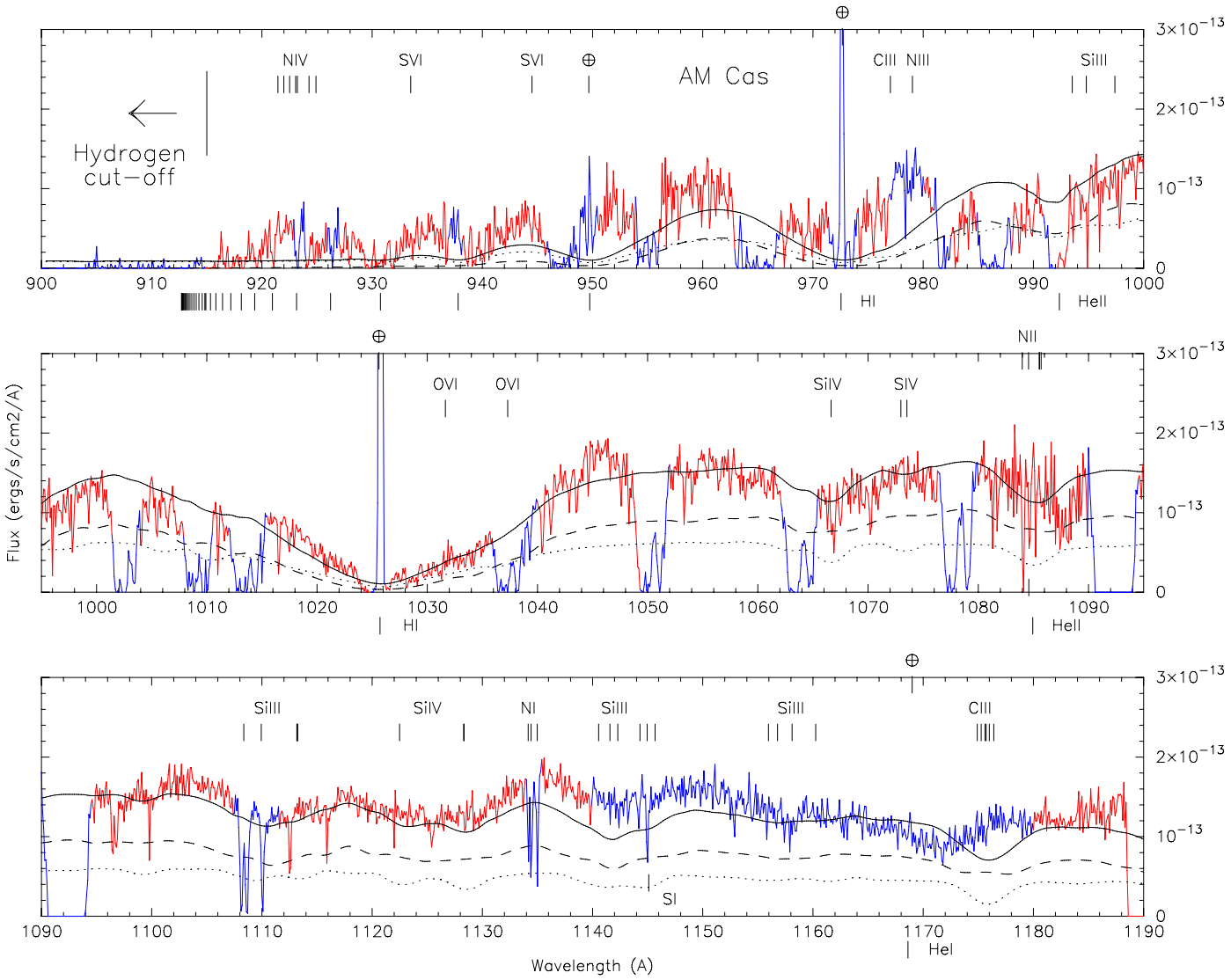

Figure 10. Best fit model (the solid black line) to the *FUSE* spectrum of AM Cas (in light gray/red) assuming $E(B-V) = 0.0$ is a WD+disk composite model. The regions that have been masked before fitting are shown in dark gray (blue). The WD model (the dotted line) has $M = 0.8\,M_{\odot}$, $T = 36{,}000$ K, $V_{\rm rot} \sin i = 500$ km s^{-1}, and the disk model (the dashed line) has a mass accretion rate $\dot{M} = 2 \times 10^{-10}\,M_{\odot}$ yr^{-1} and an inclination $i = 18^{\circ}$. This model gave a distance of 373 pc, $\chi^2 = 0.563$, with the WD contributing 41% of the flux and the disk 59%.

(A color version of this figure is available in the online journal.)

the WD model to about 40,000 K. This in turn increases the distance to $d > 400$ pc and $\chi^2 > 0.57$. We note that performing the same WD+disk composite model fit with a lower mass gave about the same results but with a larger distance, while a larger mass gave a smaller distance. However, we do not consider these models here as we used a distance in agreement with the distance obtained using the period–magnitude relations of Warner (1987) and Harrison et al. (2004), namely $d \approx 350$ pc (see Table 3).

$E(B-V) = 0.2$. We performed the same model fits. The best-fit model is a WD+disk composite model with $M = 0.55\,M_{\odot}$, $\dot{M} = 3 \times 10^{-9}\,M_{\odot}$ yr^{-1}, an inclination $i = 18^{\circ}$, a WD temperature $T = 35{,}000$ K with a projected rotational velocity $V_{\rm rot} \sin i = 400$ km s^{-1}. The distance obtained is 331 pc, $\chi^2 = 0.538$, with the WD contributing only 11% of the flux and the disk 89% (Figure 11). This model does better at fitting the spectrum both at the shorter and longer wavelengths. However, it fits the Lyβ region a little less well. The higher mass models do not perform as well and give a distance $d <$ 250 pc.

4.2.2. FO Persei/22.1939

FO Per has a mean outburst cycle of about 10 days (Howarth 1976; Gessner 1978) and belongs to those DNs with a particularly high outburst rate. Its magnitude varies between 11.8 and 16.2 (Downes et al. 2001). It was observed in the optical by Bruch et al. (1987) and Bruch (1989), but these and more recent observations have not been able to unambiguously determine the orbital period of the system: it is not clear whether the period is 3.52 hr or 4.13 hr (Sheets et al. 2007). However, with these values, we assess the distance to FO Per using the absolute outburst magnitude/Period relation (Warner 1987; Harrison et al. 2004; see Table 3) and we obtain $d \approx 270$ pc.

FO Per was observed with *FUSE* on 2007 February 11 (JD2454142.1) and the AAVSO data indicate that it was caught in an intermediate state of brightness at 13.4 mag. The *FUSE*

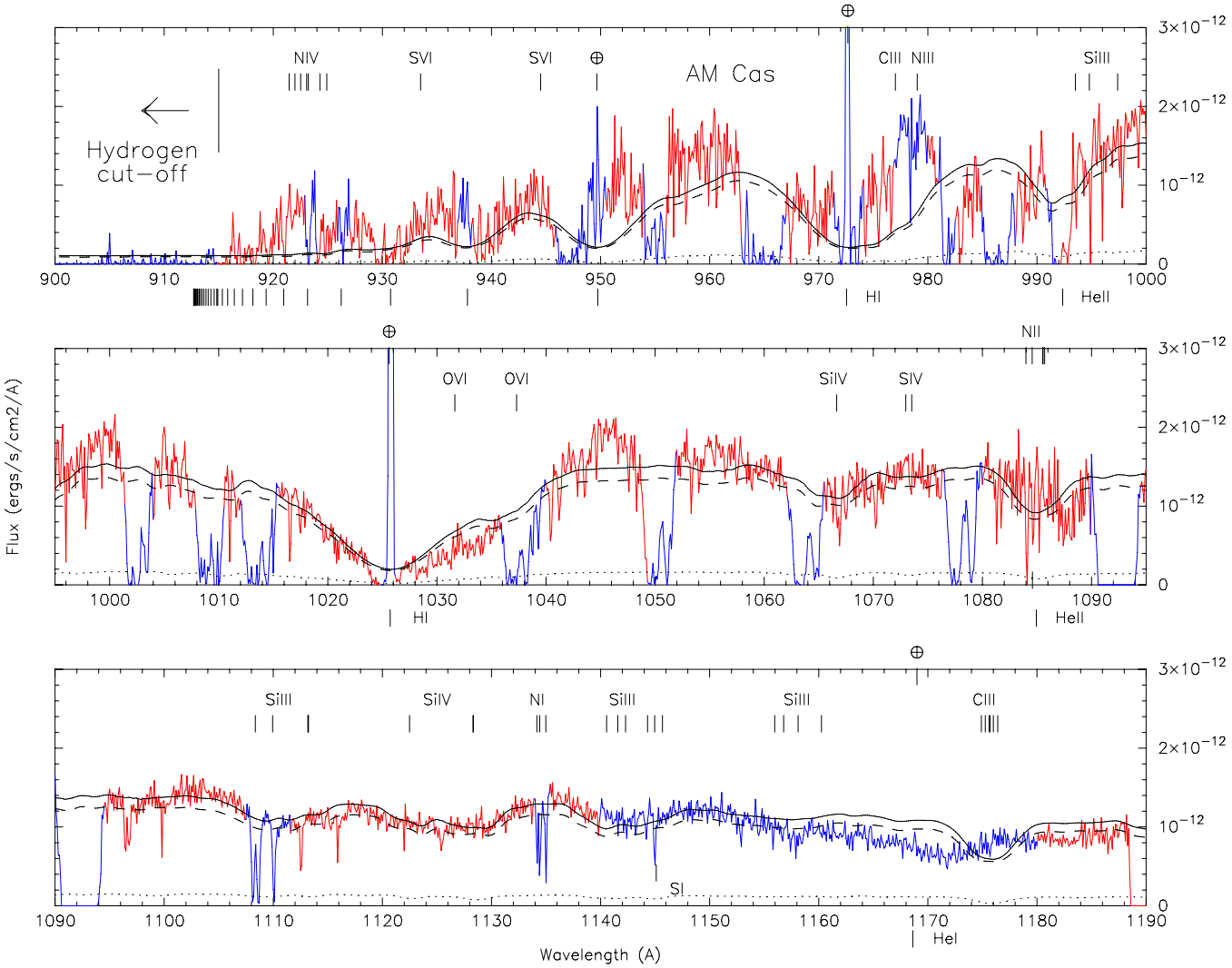

Figure 11. Best-fit model (the solid black) to the *FUSE* spectrum of AM Cas assuming $E(B-V) = 0.2$ is a WD+disk composite model. The WD model (the dotted line) has $M = 0.55\,M_{\odot}$, $T = 35{,}000$ K, $V_{\rm rot} \sin i = 400$ km s^{-1}, and the disk model (the dashed line) has a mass accretion rate $\dot{M} = 3 \times 10^{-9}\,M_{\odot}\ ^{-1}$yr and an inclination $i = 18^{\circ}$. This model gave a distance of 331 pc, $\chi^2 = 0.538$, with the WD contributing 11% of the flux and the disk 89%. The excess flux in the shorter wavelengths could be due to emission from N IV and S VI. There seems to be some broad C III (977 Å) and N III (980 Å) emission, while the higher flux around ∼950–962 Å cannot be accounted for. In the lower panel the Si III (1108–1113 Å), Si IV (1123 and 1128 Å), and Si III (1140–1145 Å) lines are broadened (Keplerian motion) and are identified as the depression in the flux there. The Si III (∼1158 Å) and C III (1175 Å) are not identified, possibly due to the deterioration of the spectra in the region of the worm.

(A color version of this figure is available in the online journal.)

spectrum of FO Per is of moderately good quality, exhibiting both interstellar (molecular hydrogen) and intrinsic absorption features (see Figure 12). There is definitely more flux in the longer wavelengths: this is a sign of either a strong reddening or a moderate temperature. Except for airglow, there are no emission lines.

Even though FO Per was caught with *FUSE* while reaching 13.4 mag (brighter than AM Cas at 13.8 mag), it has a continuum FUV flux level three times lower than that of AM Cas; namely, at the time of the observations FO Per was *redder* than AM Cas. This is consistent with the fact that the Galactic reddening in the direction of FO Per is extremely large, namely $E(B-V) = 1.78$, as the dust reddening in the direction of the constellation of Perseus is quite large. To estimate the reddening of FO Per, we note (Table 3) that TZ Per has a known reddening of 0.27 at a distance of about 500 pc, with a Galactic reddening of 0.8. Since FO Per is about half this distance but with a Galactic reddening about twice as large, we assume that the reddening of FO Per is about 0.3. We carry out simulations assuming both $E(B-V) = 0.0$ and $E(B-V) = 0.3$ to assess the effect of the reddening on the results.

$E(B-V) = 0.0$. For the single disk models, we find little agreement between the models and the observed spectra. Assuming $M = 0.4\,M_{\odot}$, we find a mass accretion rate $\dot{M} = 10^{-8.5}\,M_{\odot}$ yr^{-1}; while for the larger mass models $M = 1.2\,M_{\odot}$ the mass accretion rate decreases to a quiescent value $10^{-10.5}\,M_{\odot}$ yr^{-1}. Next, we try the single WD models and find that they do not provide a better fit. The lower mass models have a temperature of ∼25,000 K, and the higher mass models have a temperature of up to 45,000 K. Because of the rather poor fit, the rotational velocity does not influence the results, and we find that the 200 km s^{-1} models are about as good as the 400 km s^{-1} models. We then run the combined WD+disk model fits and find the best fit to be for

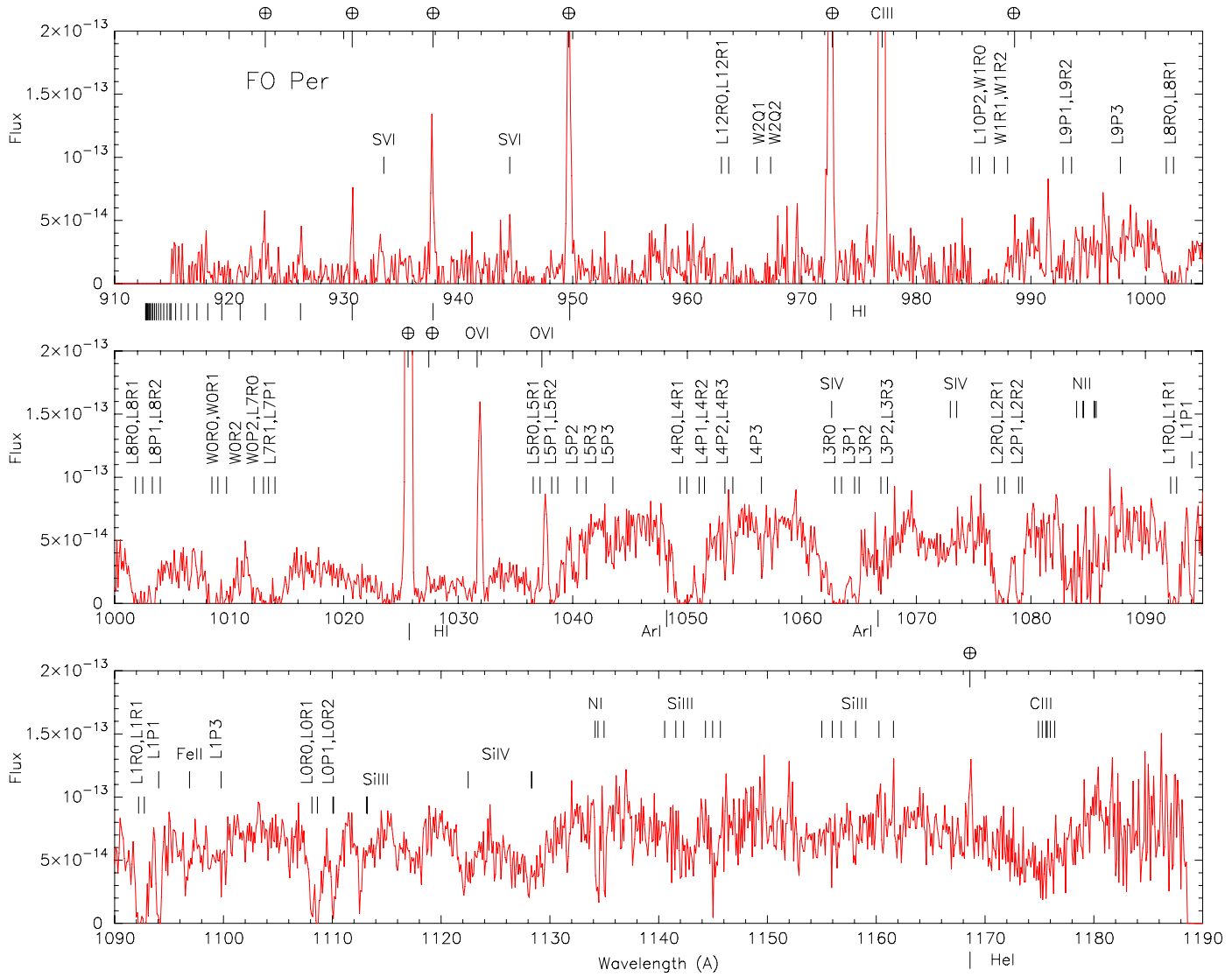

Figure 12. *FUSE* spectrum of FO Per. All the sharp emission lines are due to geo- and heliocoronal contamination, including the S VI and O VI lines. All the ISM hydrogen molecular absorption lines have been annotated vertically. The broad Lyβ feature is visible, as well as the broad carbon (C III 1175 Å) and silicon (Si III 1113 Å, Si IV 1123 and 1128 Å, Si III ∼1140–1145 Å) absorption features. All the other metal lines have not been identified, but have been marked for comparison.
(A color version of this figure is available in the online journal.)

a 0.4 $M_\odot$ WD mass, with T_{wd} = 21,000 K, $V_{\rm rot} \sin i$ = 200 km s^{-1}, i = 75°, $\dot{M}$ = $10^{-8.5}$ $M_\odot$ yr^{-1}, d = 291 pc, and the least χ^2 is 0.258. The WD contributes 29% of the FUV flux, while the disk contributes 71%. This model is shown in Figure 13.

$E(B-V) = 0.3$. The best-fit single disk model has M_{wd} = 1 $M_\odot$, i = 18°, $\dot{M}$ = 10^{-9} $M_\odot$ yr^{-1}, and gives a distance of 281 pc and a much smaller χ^2, namely 0.172. The single WD model gives not only a smaller χ^2 but also a much smaller distance. For a 0.4 $M_\odot$ WD mass, the best fit has a temperature T_{wd} = 35,000 K, a rotational velocity of 200 km s^{-1}, and gives a distance of 135 pc and χ^2 = 0.152. For larger WD masses, we find an even smaller distance and we, therefore, disregard the single WD models. We then try the combined WD+disk models and find that a valid distance of 254 pc is obtained for a 0.4 $M_\odot$ WD mass, with T_{wd} = 40,000 K, $V_{\rm rot} \sin i$ = 200 km s^{-1}, i = 18°, $\dot{M}$ = $10^{-8.5}$ $M_\odot$ yr^{-1}, and this best model gives the least χ^2 of all 0.146. The WD contributes 52% of the FUV flux, while the disk contributes the remaining 48%. This model is shown in Figure 14.

4.2.3. ES Draconis/Dra3/PG 1524+622

ES Dra has a magnitude varying between 13.9 and 16.3 (Andronov 1991; Downes et al. 2001). First suspected to be a CV by Green et al. (1986), it is classified as a SU UMa system by Downes et al. (2001), and the nondetection of prominent superhumps indicates that it might have a low inclination (Andronov et al. 2003). However, its orbital period of 4.29 hr (Ringwald 1994) makes its classification as a SU UMa unlikely. ES Dra appears to sit about 1 mag below outburst for months, which is more characteristic of Z Cam systems. We, therefore, tentatively classify ES Dra as a Z Cam, and this classification is also consistent with its location above the period gap.

ES Dra was observed with *FUSE* on 2006 November 19 (JD2454059). However, no AAVSO data were collected around

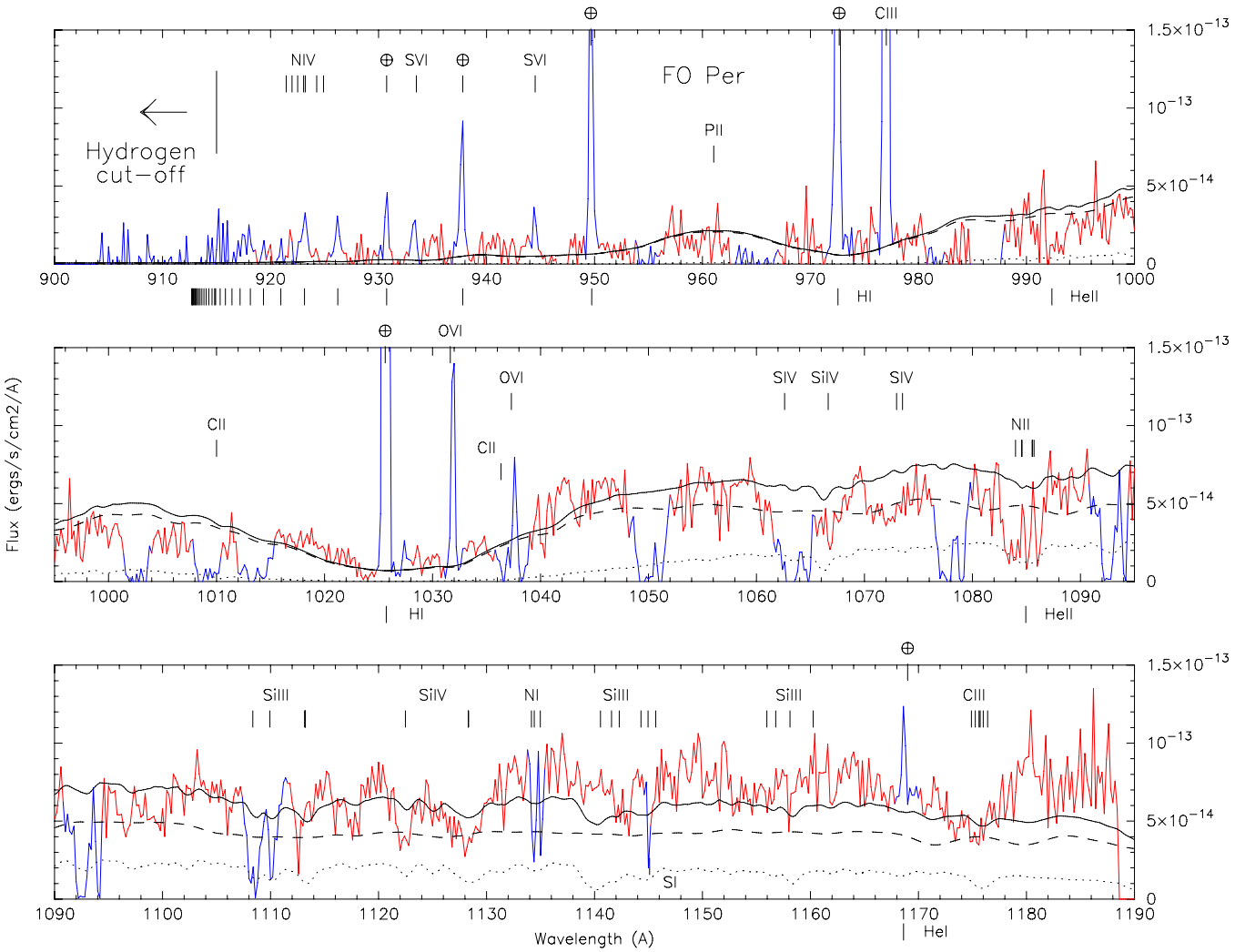

Figure 13. Best-fit WD+disk composite model (the solid black) to the *FUSE* spectrum of FO Per assuming $E(B-V) = 0.0$. The observed spectrum is in red (light gray) and the regions that have been masked for the fitting are in blue (dark gray). The WD model (the dotted line) has 0.4 $M_{\odot}$, with $T_{wd} = 21{,}000$ K, and $V_{\rm rot} \sin i$ =200 km s^{-1}, the disk model (the dashed line) has $i = 75°$, and $\dot{M} = 10^{-8.5}\,M_{\odot}$ yr^{-1}. The distance obtained is $d = 291$ pc with $\chi^2 = 0.258$. The WD contributes 29% of the FUV flux, while the disk contributes 71%.

(A color version of this figure is available in the online journal.)

the period of the actual *FUSE* observation. From the *FUSE* continuum flux level (2×10^{-14} erg s^{-1} cm^{-2} Å^{-1}), it seems that ES Dra must have been in an intermediate (standstill) state, possibly at 15.0–15.4 mag, where the heated WD might be the main component of the FUV continuum. The spectrum of ES Dra is shown in Figure 15.

The C III (1175) multiplet possibly exhibits a P-Cygni profile, where the broad absorption line is blueshifted by about 3 Å, and the broad emission line is redshifted by about the same amount. This corresponds to a velocity of about ∼750 km s^{-1}. Such a high velocity is probably originating close to the WD/inner disk. The C III (977) broad emission line is also redshifted by at least 2 Å. The two broad S IV absorption lines (∼1063+1073) are blueshifted by 2 Å, while the Si III+IV (∼1110+1125) broad absorption features also show a slight blueshift. It is clear that the C III and S IV lines are forming in an expanding shell or a corona, while the Si absorption feature also forms in the disk and atmosphere of the WD. We therefore decided to mask the C III and S IV lines in the model fitting, while keeping the Si lines.

We assume that the reddening toward ES Dra is negligible as the Galactic (maximum) reddening in that direction is itself very small: 0.03. The distance to the system inferred from the period–magnitude relation is 770 pc (see Table 3), and this is the distance we use in the modeling.

Single Disk Models. The lowest χ^2 model in best agreement with a distance of 770 pc is for $M = 1.2\,M_{\odot}$, $\dot{M} = 10^{-10}\,M_{\odot}$ yr^{-1}, which gives a distance of 1035 pc and $\chi^2 > 0.57$. The fit can be improved by changing the abundances; namely the silicon and sulfur broad absorption features are best fit when Si ≈ 10× solar and S ≈ 50× solar. The fit is further improved (lower χ^2) by blueshifting the entire synthetic spectrum by 1.0 Å. This best single disk model gave a distance of 1754 pc and $\chi^2 = 0.4280$. This model is shown in Figure 16.

Single White Dwarf Models. We tried to fit both the distance (770 pc) and the higher order of the Ly series. We first tried solar abundances models and then increased the silicon and sulfur abundances to better fit the silicon and sulfur absorption features. The best model (Figure 17) has $T = 35{,}000$ K, $\log(g) = 7.8$ (corresponding to $M_{wd} \approx 0.58\,M_{\odot}$), a projected

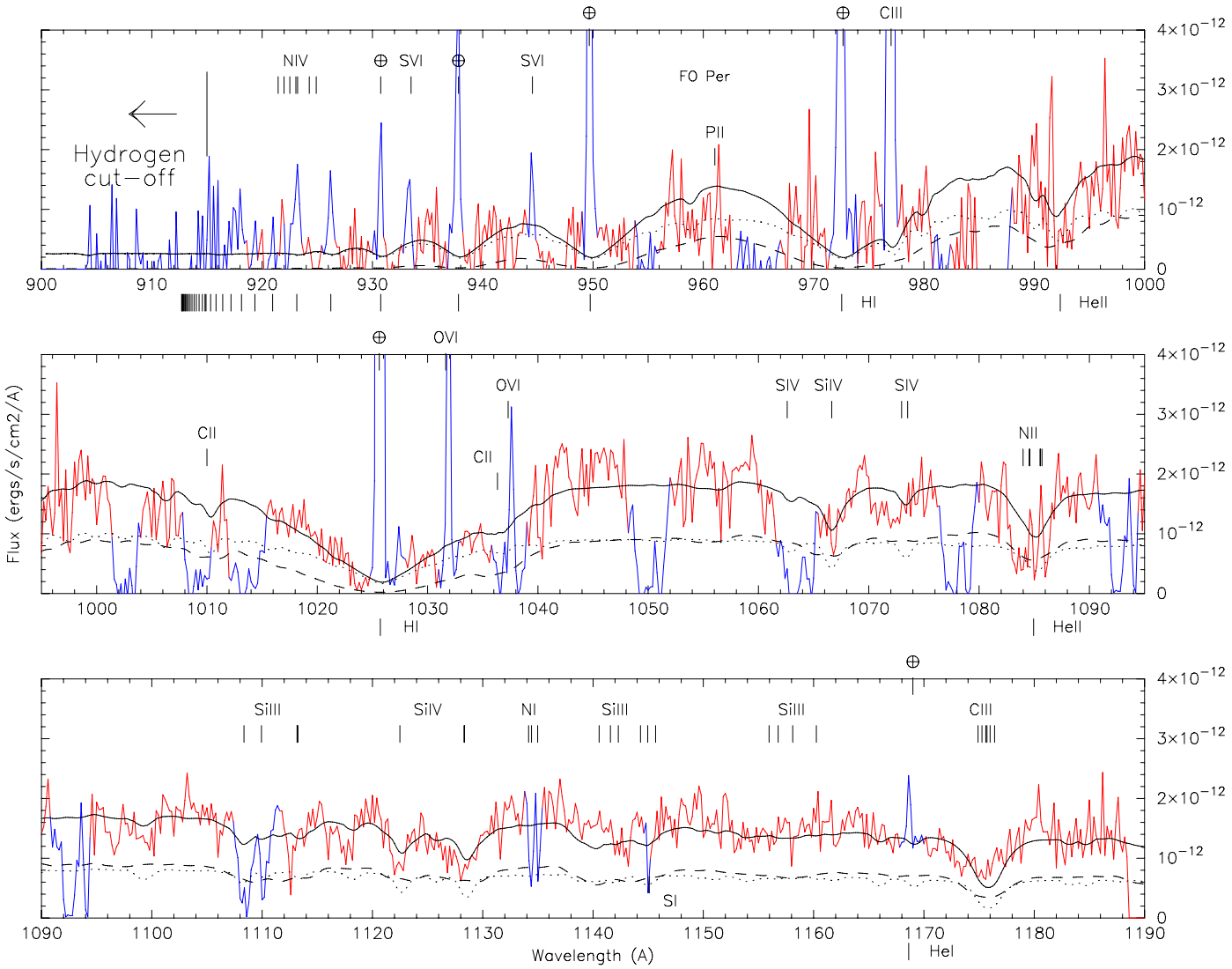

Figure 14. Best-fit WD+disk composite model to the dereddened *FUSE* spectrum of FO Per assuming $E(B-V) = 0.3$. The WD model (the dotted line) has a 0.4 $M_\odot$ and $T_{wd} = 40{,}000$ K, and $V_{\rm rot} \sin i = 200$ km s^{-1}. The disk model (the dashed line) has $i = 18^\circ$, and $\dot{M} = 10^{-8.5}$ $M_\odot$ yr^{-1}. The model gives a distance $d = 254$ pc with $\chi^2 = 0.146$. The WD contributes 52% of the FUV flux, while the disk contributes 48%. When compared with the model, we find that the C III (1175 Å) and Si IV (1123, 1128 Å) lines are blueshifted by ∼2 Å and ∼1 Å, respectively. The S IV (1063,1073 Å) lines might also be blueshifted.

(A color version of this figure is available in the online journal.)

rotational velocity $v_{\rm rot} \sin i = 700$ km s^{-1}. Here too, we find that the best fit is obtained with Si $\approx 10\times$ solar, $S \approx 50\times$ solar, and a blueshift of 1.3 Å. The distance obtained is 773 pc and $\chi^2 = 0.4277$. From the point of view of the least χ^2, this model is as good as the least χ^2 single disk model; however, the distance is in much better agreement with the estimate of 770 pc (Table 3).

We find that WD+Disk composite models do not improve the fit, but rather the opposite.

5. SUMMARY

We report the results of a spectroscopic analysis of a *FUSE* survey of high-declination DNs, including five southern hemisphere objects and three northern hemisphere objects. In order to model these spectra, we assessed the distance and reddening of these objects and carried out a synthetic spectral fit to the observed spectra.

The low S/N in some of the spectra prevented us from obtaining robust results: for AQ Men and V433 Ara, we were only able to assess a lower limit for the WD temperature or mass accretion rate. Though we were unable to assess their distance, for HP Nor we found a WD temperature of about 40,000 K and rotational velocity of 1000 km s^{-1}, and for DT Aps we found a WD temperature of at least 34,000 K and a rotational velocity of 500 km s^{-1}.

For the four objects with relatively good spectra, we were able to obtain more reliable results. For NSV 10934 we find a low-mass accretion rate, high-inclination angle, and a large WD mass. For AM Cas the best-fit model is a WD+disk composite model with a low inclination, a WD temperature $T = 35{,}000$ K, a mass 0.55 $M_\odot$, and a mass accretion rate of 3×10^{-9} $M_\odot$ yr^{-1}. For FO Per the best fit is also a WD+ disk composite model giving $M = 0.4\,M_\odot$, $T = 40{,}000$ K, a low inclination and a mass accretion rate consistent with outburst ($10^{-8.5}$ $M_\odot$ yr^{-1}). And for ES Dra the spectrum is best fit with a single WD stellar atmosphere with $T = 35{,}000$ K, $M = 0.58\,M_\odot$, and a projected rotational velocity of 700 km s^{-1} with overabundant silicon and sulfur.

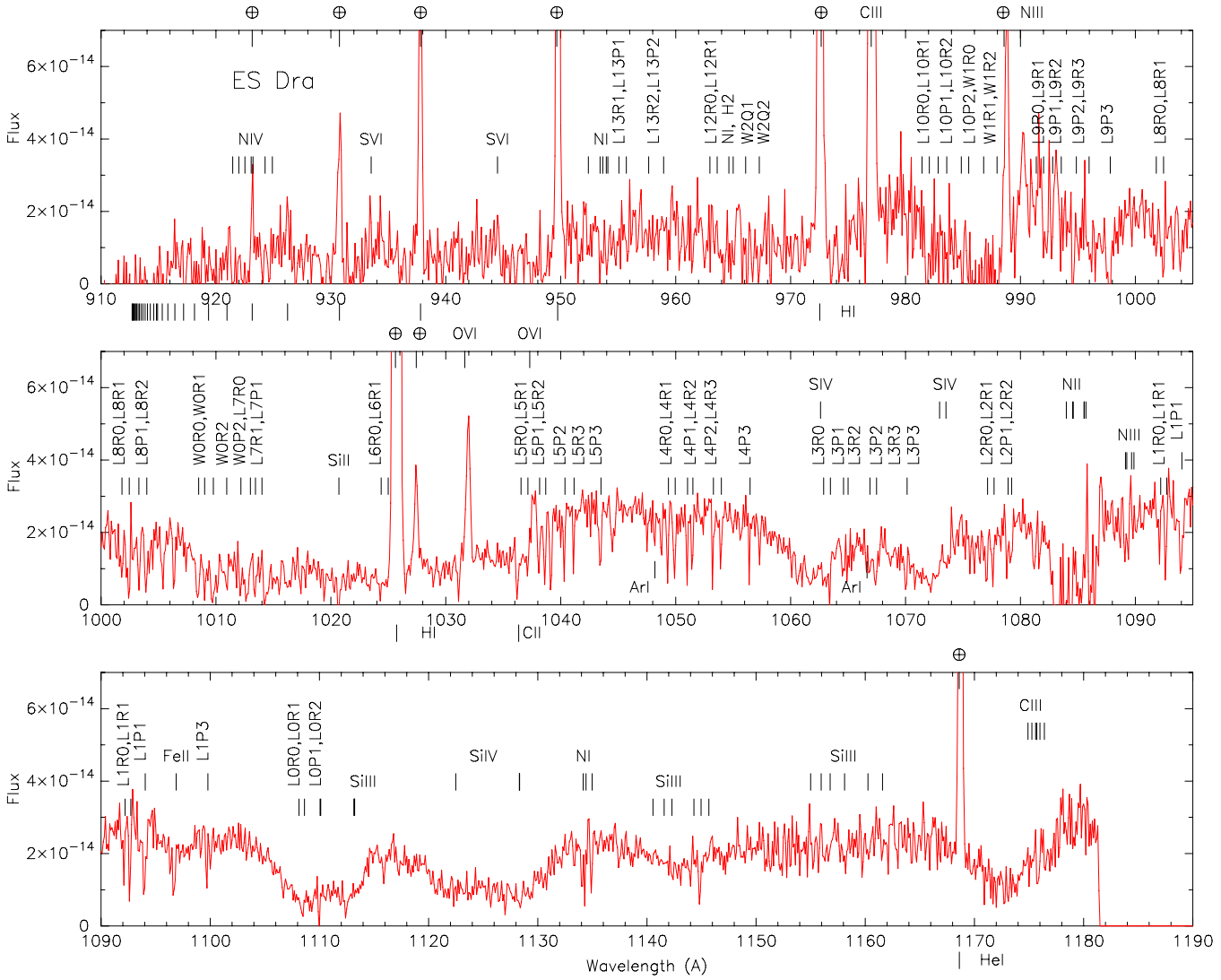

Figure 15. *FUSE* spectrum of ES Dra with line identifications. All the sharp emission lines are due to geo- and heliocoronal contamination, including the S VI, O VI, and C III (977 Å) lines. Broad absorption features from carbon and silicon are clearly seen, slightly blueshifted. The shifting of the lines is more apparent in Figures 16 and 17, where the observed spectrum is compared with the models.

(A color version of this figure is available in the online journal.)

For three objects above the period gap (AM Cas, FO Per, and ES Dra), we have found a WD temperature during an active state (intermediate-to-outburst) reaching 35,000–40,000 K. These must be regarded as an upper limit as the WD was heated due to ongoing (or recent) accretion. These temperatures are similar to the temperature of RX And on the rise to outburst (39,000 K) and in decline from outburst (45,000 K), while in quiescence its temperature is 34,500 K (Sepinsky et al. 2002). It is therefore likely that the true temperatures of AM Cas, FO Per, and ES Dra in quiescence are around 30,000–35,000 K, and these objects are therefore near the average CV WD's $T_{\rm eff}$ above the period gap (∼30,000 K), similar to U Gem, SS Aur, and RX And.

We have recapitulated the effective quiescent CV WD temperatures as found in the literature in Table 5. The references are listed in the last column. Similar tables are given in the literature (Townsley & Gänsicke 2009) and sometimes reflect slightly different values, which is due to the fact that (1) for some of the systems, more than one model (and therefore more than one WD temperature) was given and we list here the best fit in which the WD contributes more than 50% of the flux, and (2) we also list the most recent synthetic spectral fits obtained by our own group. For WZ Sge and VW Hyi, a theoretical cooling curve of the WD was computed to fit the observed temperature decline in these systems: the quiescent temperature was the asymptotic value approached as $t \rightarrow \infty$. The temperatures listed in Table 5 are depicted in Figure 18, from which there seems to be a clear separation between Polars and DNs, both above and below the gap (Araujo-Betancor et al. 2003). VY Scl systems also seem definitely hotter than DNs. It is evident from this figure that more data points are badly needed for Z Cam systems as well as for all the CV subtypes above the gap, except maybe for U Gem's. The data points from the present work have been added as downward-pointing arrows, as they are only upper limits. Since the mass and the distance are not known with accuracy for many of the systems listed in Table 5, it is very likely that some of the temperatures in Table 5 will change once parallaxes and/or masses are obtained for these systems. The standard model above the gap (traditional magnetic braking; Howell et al. 2001) is between the dotted lines.

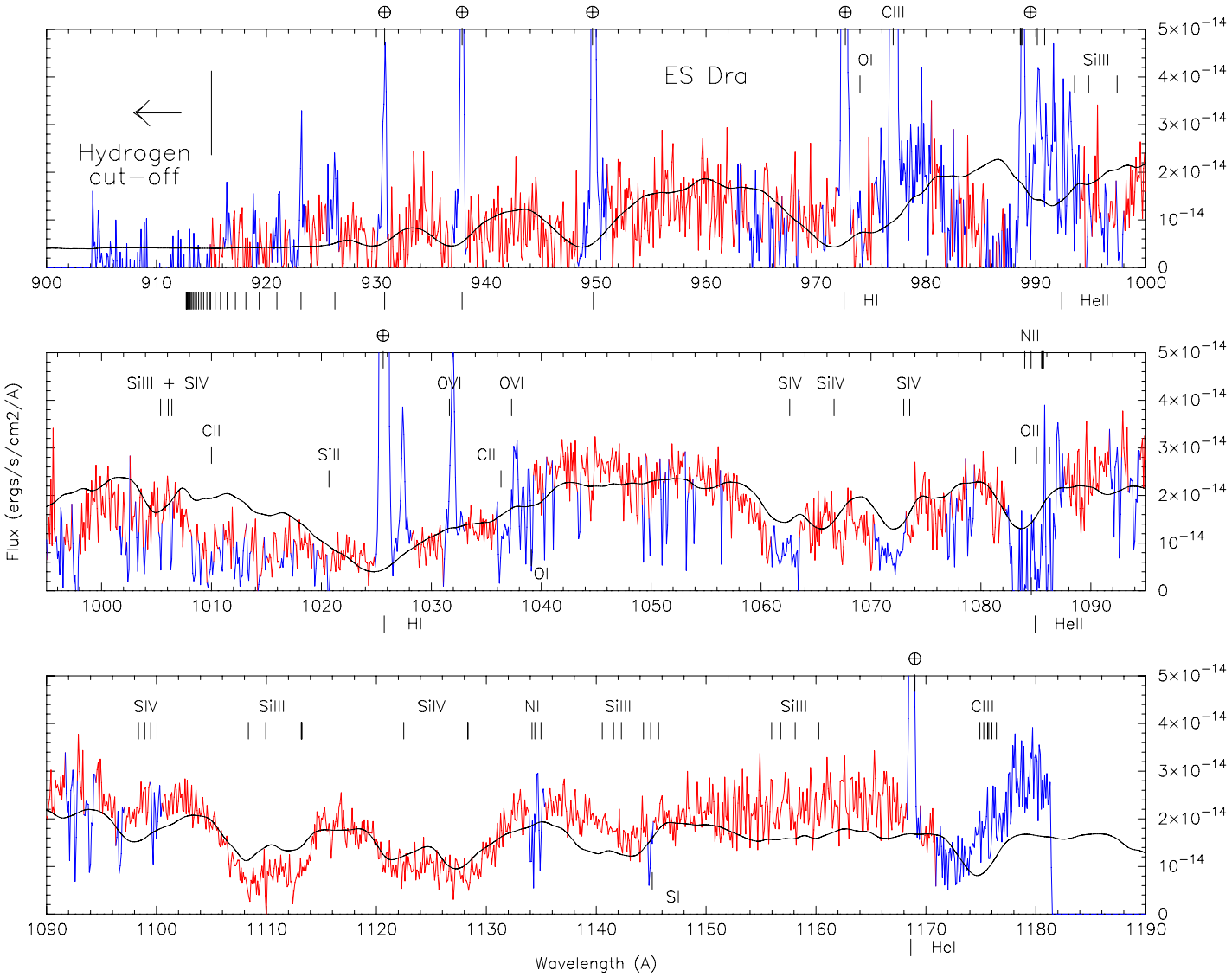

Figure 16. Best-fit accretion disk model to the *FUSE* spectrum of ES Dra. The regions of the spectrum that have been masked for the fitting are in blue. The disk model has a central accreting WD with a mass $M = 1.2\,M_{\odot}$, a mass accretion rate $\dot{M} = 10^{-9.5}\,M_{\odot}\ \mathrm{yr}^{-1}$, and an inclination $i = 5^{\circ}$, and gives a distance of 1754 pc. We fine-tuned the fitting by setting the silicon and sulfur abundances 10× solar and 50× solar, respectively. We also shifted the entire synthetic spectrum to the blue by 1.0 Å. This resulted in $\chi^2 = 0.4280$.

(A color version of this figure is available in the online journal.)

The recent work of Townsley & Gänsicke (2009) recapitulates and analyzes the effective temperatures of the WD in CVs; therefore, we wish only to emphasize the (small) differences that we obtain above the period gap when considering the values given in Table 5. We include in the present work more data points for the VY Scl systems (BB Dor, V794 Aql, VY Scl) and DNs, and we also draw systems with $P > 5$ hr. Since we use the same data points for the magnetic systems, we agree that gravitational radiation can account for the WD $T_{\rm eff}$ (and therefore $\dot{M}$) of polars both above and below the gap. Above the gap we also agree that the majority of DNs have a temperature (mass accretion rate) lower than expected by the standard theory, and that NL VY systems have a temperature higher than expected from the standard theory. However, we find that the traditional magnetic braking could explain the temperature (mass accretion rate) of some systems (TU Men, BB Dor, SS Aur, U Gem) above the period gap.

Overall, it seems that the standard model (and any modified model; see Townsley & Gänsicke 2009 for a discussion) does not agree with the nonmagnetic CVs above the period gap. While it is difficult to explain the discrepancy above the gap between the theory and observations for the DN systems, a higher than expected temperature for the NL VY can be accounted for with a higher mass accretion rate $\langle \dot{M} \rangle$.

P.G. wishes to thank Mario Livio for his kind hospitality at the Space Telescope Science Institute, where part of this work was carried out. We wish to thank the members of the American Association of Variable Star Observers (AAVSO), the Austral Variable Star Observer Network (AVSON), and the Center for Backyard Astrophysics (CBA) for providing us with optical monitoring of northern and southern hemisphere systems, as well as optical archival data on these systems. This research was based on observations made with the NASA–CNES–CSA

Table 5
CV WD Temperatures in Quiescence

Name[a]	Type	P_{orb} (minutes)	T_{wd} (K)	References
GW Lib	DN SU	76.8	13,300	Szkody et al. (2002a)
BW Scl	DN SU	78.2	14,800	Gänsicke et al. (2004)
LL And	DN SU	79.2	14,300	Howell et al. (2002)
EF Eri	NL AM	81.0	9,500	Beuermann et al. (2000)
WZ Sge	DN SU	81.6	13,500	Godon et al. (2006b)
AL Com	DN SU	81.6	16,300	Szkody et al. (2003)
SW UMa	DN SU	81.8	14,000	Gänsicke et al. (2004); Urban & Sion (2006)
HV Vir	DN SU	83.5	13,300	Szkody et al. (2002b)
WX Cet	DN SU	83.9	14,500	Sion et al. (2003); Urban & Sion (2006)
T Leo	DN SU	84.7	16,000	Hamilton & Sion (2004)
EG Cnc	DN SU	86.4	13,300	Szkody et al. (2002b)
DP Leo	NL AM	89.8	13,500	Schwope et al. (2002)
V347 Pav	NL AM	90.0	12,300	Araujo-Betancor et al. (2005)
BC UMa	DN SU	90.2	15,200	Gänsicke et al. (2004); Urban & Sion (2006)
VY Aqr	DN SU	90.8	14,000	Sion et al. (2003); Urban & Sion (2006)
EK TrA	DN SU	91.6	17,000	Godon et al. (2008a)
BZ UMa	DN SU	97.9	17,500	P. Godon (2007, unpublished); Urban & Sion (2006)
VV Pup	NL AM	100.4	12,100	Araujo-Betancor et al. (2005)
V834 Cen	NL AM	101.5	14,200	Araujo-Betancor et al. (2005)
HT Cas	DN SU	106.1	18,000	Urban & Sion (2006)
VW Hyi	DN SU	106.9	19,000	E. M. Sion & P. Godon (2009, in preparation)
CU Vel	DN SU	113.0	18,500	Gänsicke & Koester (1999)
BL Hyi	NL AM	113.6	13,100	Araujo-Betancor et al. (2005)
MR Ser	NL AM	113.5	14,000	Araujo-Betancor et al. (2005)
ST LMi	NL AM	113.9	10,800	Araujo-Betancor et al. (2005)
EF Peg	DN SU	123.0	16,600	Howell et al. (2002)
HU Aqr	NL AM	125.0	14,000	Gänsicke (1999)
UV Per	DN SU	125.0	20,000	Urban & Sion (2006)
QS Tel	NL AM	139.9	17,500	Rosen et al. (2001)
TU Men	DN UG	168.8	28,000	Sion et al. (2008)
AM Her	NL AM	185,6	19,800	Gänsicke et al. (2006)
MV Lyr	NL VY	191.0	47,000	Hoard et al. (2004)
DW UMa	NL SW	196.7	50,000	Araujo-Betancor et al. (2003)
TT Ari	NL VY	198.0	39,000	Gänsicke et al. (1999)
BB Dor	NL VY	214.8	32,000	Godon et al. (2008b)
V794 Aql	NL VY	220.8	47,000	Godon et al. (2007)
UU Aql	DN UG	235.5	27,000	Sion et al. (2007)
X Leo	DN UG	237.0	33,000	Urban & Sion (2006)
AM Cas	DN ZC	237.6	<35,000	This work
VY Scl	NL VY	239.3	45,000	Hamilton & Sion (2008)
FO Per	DN UG	229.5[a]	<40,000	This work
V1043 Cen	NL AM	251.4	15,000	Gänsicke et al. (2000)
WW Cet	DN	253.1	26,000	Godon et al. (2006a)
U Gem	DN UG	254.7	31,000	Sion et al. (1998); Long & Gilliland (1999); Urban & Sion (2006)
ES Dra	DN ZC	257.4	<35,000	This work
SS Aur	DN UG	263.2	34,000	Godon et al. (2008a)
V895 Cen	NL AM	285.9	13,800	Araujo-Betancor et al. (2005)
RX And	DN ZC	302.2	34,000	Sion et al. (2001); Urban & Sion (2006)
TT Crt	DN UG	386.4	30,000	Sion et al. (2008); Urban & Sion (2006)
SS Cyg	DN UG	396.2	55,000	Sion et al. (2007)
Z Cam	DN ZC	417.4	57,000	Hartley et al. (2005)
RU Peg	DN UG	539.4	70,000	Godon et al. (2008a)
EY Cyg	DN UG	661.4	30,000	Godon et al. (2008a)
V422 Cen	DN UG	662.4	47,000	Sion et al. (2008)
BV Cen	DN UG	878.6	40,000	Sion et al. (2007)

Note.
[a] For FO Per it is not known whether the period is 211.2 minutes or 247.8 minutes; we, therefore, took the intermediate value 229.5 minutes for practical reasons.

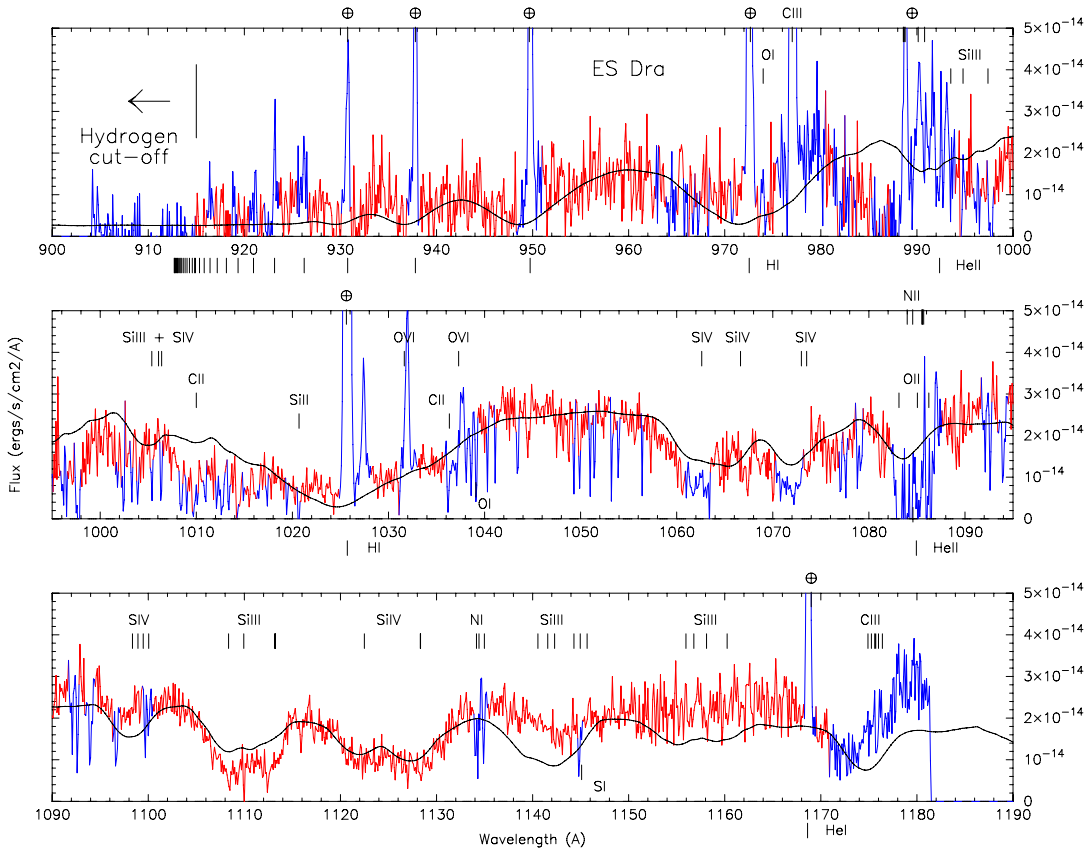

Figure 17. Best-fit single component WD model to the *FUSE* spectrum of ES Dra. The WD has a temperature $T = 35{,}000$ K, $\log(g) = 7.8$ (corresponding to $M_{wd} \approx 0.58\,M_{\odot}$), a projected rotational velocity $v_{\rm rot} \sin i = 700$ km s^{-1}, abundances Si $\approx 10\times$ solar, S $\approx 50\times$ solar and a blueshift of 1.3 Å. This model gives a distance of 773 pc and $\chi^2 = 0.4277$. When compared with the synthetic spectrum, the observed spectrum clearly reveals the Si III (∼1110 Å) and Si IV (1023 and 1028 Å) lines; the Si III lines in the longer wavelengths do not match the model. The C III (1175 Å) presents a P-Cygni profile; the S IV (1063, 1073, and 1099 Å) lines are blueshifted. The Si III + S IV (∼1006 Å), C II (1010 Å), Si IV (1066 Å) lines are all contaminated with ISM absorption (see Figure 15 for comparison).

(A color version of this figure is available in the online journal.)

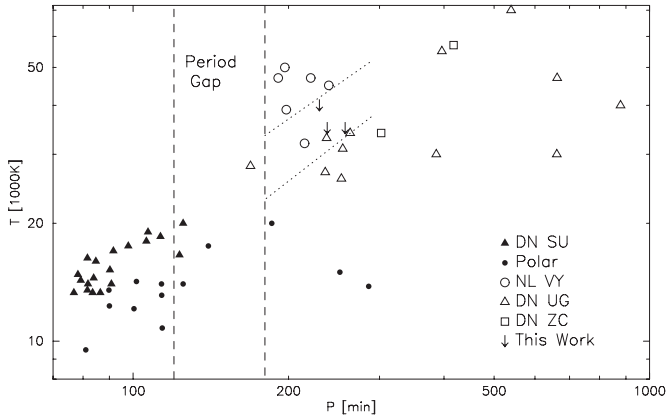

Figure 18. Effective white dwarf temperature as a function of the orbital period from Table 5. There is a well defined separation between Polars and DNs below the gap, and apparently also above the gap. There is clearly a lack of data points above the gap for Z Cam's, Polars, and VY Scl's. There seems to be a separation in the $P - T_{\rm eff}$ parameter space between Polars, SU UMa's, U Gem's, and possibly VY Scl's. The three arrows (this work) are only upper limits and have been included here to show how important it is to obtain good FUV spectra and parallax for CVs in order to be able to derive robust results for the WD effective temperatures. The traditional magnetic braking above the period gap (Howell et al. 2001) is shown between the dotted lines.

Far Ultraviolet Spectroscopic Explorer. *FUSE* is operated for National Aeronautic and Space Administration (NASA) by the Johns Hopkins University under NASA contract NAS5-32985. This work was supported by the NASA under *FUSE* Cycle 7 (Guest Investigator Program) grant NNX06AD28G and supported in part by NSF grant AST0807892, both to Villanova University. This publication also makes use of the data products from the Two Micron All Sky Survey, which is a joint project of the University of Massachusetts and the Infrared Processing and Analysis Center/California Institute of Technology, funded by the NASA and the National Science Foundation.

REFERENCES

Andronov, I. L. 1991, Inf. Bull. Variable Stars, 3645
Andronov, I. L., et al. 2003, in ASP Conf. Ser. 292, Interplay of Periodic, Cyclic and Stochastic Variability in Selected Areas of the H-R Diagram, ed. C. Sterken (San Francisco, CA: ASP), 313
Andronov, N., Pinsonneault, & Sills, A. 2003, ApJ, 582, 358
Araujo-Betancor, S., et al. 2003, ApJ, 583, 437
Araujo-Betancor, S., Gänsicke, B. T., Long, K. S., Beuermann, K., de Martino, D., Sion, E. M., & Szkody, P. 2005, ApJ, 622, 589
Basri, G. 1987, ApJ, 316, 377
Beuermann, K., Wheatley, P., Ramsay, G., Euchner, F., & Gänsicke, B. T. 2000, A&A, 354, L49
Bruch, A., & Engel, A. 1994, A&AS, 104, 79
Bruch, A. 1989, A&AS, 78, 145
Bruch, A., et al. 1987, A&A, 70, 481
Cheng, A., O'Donoghue, D., Stobie, R. S., Kilkenny, D., & Warner, B. 2001, MNRAS, 325, 89
Clemens, C. J., Reid, N. I., Gizis, J. E., & O'brian, S. M. 1998, ApJ, 496, 352
Dixon, W. V., et al. 2007, PASP, 119, 527
Downes, R. A., Webbink, R. F., Shara, M. M., Ritter, H., Kolb, U., & Duerbeck, H. W. 2001, PASP, 113, 764
Eggleton, P. P. 1976, in IAU Symp. 73, Structure and Evolution of Close Binary Systems, ed. P. Eggleton, S. Mitton, & J. Whelan (Dordrecht: Reidel), 209

Faulkner, J. 1971, ApJ, 170, L99
Gänsicke, B. T. 1999, in ASP Conf. Ser. 157, in Annapolis Workshop on Magnetic Cataclysmic Variables, ed. C. Hellier & K. Mukai (San Francisco, CA: ASP), 261
Gänsicke, B. T. 2005, in ASP Conf. Ser. 330, The Astrophysics of Cataclysmic Variables and Related Objects, ed. J.-M. Hameury & J.-P. Lasota (San Francisco, CA: ASP), 3
Gänsicke, B. T., Beuermann, K., de Martino, D., & Thomas, H.-C. 2000, A&A, 354, 605
Gänsicke, B. T., & Koester, D. 1999, A&A, 346, 151
Gänsicke, B. T., Long, K. S., Barstow, M. A., & Hubney, I. 2006, ApJ, 639, 1039
Gänsicke, B. T., Sion, E. M., Beuermann, K., Fabian, D., Cheng, F. H., & Krautter, J. 1999, A&A, 347, 178
Gänsicke, B. T., Szkody, P., Howell, S. B., & Sion, E. M. 2004, ApJ, 629, 451
Gänsicke, B. T., et al. 2003, ApJ, 594, 443
Gessner, H. 1978, Mitt. Veränderl. Sterne, 8, 66
Godon, P., Seward, L., Sion, E. M., & Szkody, P. 2006a, AJ, 131, 2634
Godon, P., Sion, E. M., Barrett, P. E., Hubeny, I., Linnell, A. P., & Szkody, P. 2008a, ApJ, 679, 1447
Godon, P., Sion, E. M., Barrett, P., & Szkody, P. 2007, ApJ, 656, 1092
Godon, P., Sion, E. M., Barrett, P. E., Szkody, P., & Schlegel, E. M. 2008b, ApJ, 687, 532
Godon, P., Sion, E. M., Cheng, F., Long, K. S., Gänsicke, B. T., & Szkody, P. 2006b, ApJ, 642, 1018
Green, R. F., Schmidt, M., & Liebert, J. 1986, ApJS, 61, 305
Hack, M., & La Dous, C. 1993, Cataclysmic Variables and Related Objects (NASA SP-507/US Gov. Printing Office; Greenbelt, MD: NASA)
Hamada, T., & Salpeter, E. E. 1961, ApJ, 134, 683
Hameury, J. M., King, A. R., & Lasota, J. P. 1990, MNRAS, 242, 141
Hameury, J. M., King, A. R., Lasota, J. P., & Ritter, H. 1988, MNRAS, 231, 535
Hamilton, R. T., & Sion, E. M. 2004, PASP, 116, 926
Hamilton, R. T., & Sion, E. M. 2008, PASP, 120, 165
Harrison, T. E., Johnson, J. J., McArthur, B. E., Benedict, G. F., Szkody, P., Howell, S. B., & Gelino, D. M. 2004, AJ, 127, 460
Hartely, L. E., Long, K. S., Froning, C. S., & Drew, J. E. 2005, ApJ, 623, 425
Hoard, D. W., Linnell, A. P., Szkody, P., Fried, R. E., Sion, E. M., Hubeny, I., & Wolfe, M. A. 2004, ApJ, 604, 346
Hoffmeister, C. 1929, Astron. Nachr., 234, 33
Howarth, I. D. 1976, Mitt. Veränderl. Sterne, 7, 147
Howell, S. B., Gänsicke, B. T., Szkody, P., & Sion, E. M. 2002, ApJ, 575, 419
Howell, S. B., Nelson, L. A., & Rappaport, S. 2001, ApJ, 550, 897
Hubeny, I. 1988, Comput. Phys. Commun., 52, 103
Hubeny, I., & Lanz, T. 1995, ApJ, 439, 875
Ivanova, N., & Taam, R. E. 2004, ApJ, 601, 1058
Kato, R., et al. 2002, A&A, 396, 929
Kato, R., et al. 2004, MNRAS, 347, 861
King, A. R. 1988, QJRAS, 29, 1
King, A. R., Schenker, K., & Hameury, J. M. 2002, MNRAS, 335, 513
Knigge, C. 2006, MNRAS, 373, 484
Knigge, C. 2007, MNRAS, 382, 1982
Kolb, U. 1993, A&A, 271, 149
Kolb, U., & Baraffe, I. 1999, MNRAS, 309, 1034
Kolb, U., Rappaport, S., Schenker, K., & Howell, S. B. 2001, ApJ, 563, 958
Long, K. S., & Gilliland, R. L. 1999, ApJ, 511, 916
McCormick, P., & Frank, J. 1998, ApJ, 500, 923
Mc Dermott, P. N., & Taam, R. E. 1989, ApJ, 342, 1019
Munari, U., & Zwitter, T. 1998, A&AS, 128, 277
Notni, P., & Richter, G. A. 1984, Inf. Bull. Variable Stars, 2634
Paczyński, B., & Sienkiewicz, R. 1981, ApJ, 248, L27
Paczyński, B., & Sienkiewicz, R. 1983, ApJ, 268, 825
Panei, J. A., Althaus, L. G., & Benvenuto, O. G. 2000, A&A, 353, 970
Patterson, J. 1984, ApJS, 54, 443
Patterson, J. 2002, Center for Backyard Astrophysics (New York: CBA), http://cbastro.org/communications/news/2002/march28.html
Press, W. H., Teukolsky, S. A., Vetterling, W. T., & Flannery, B. P. 1992, Numerical Recipes in Fortran 77, The Art of Scientific Computing (2nd ed.; Cambridge Univ. Press)
Pretorius, M. L., Warner, B., & Woudt, P. A. 2006, MNRAS, 368, 361
Price, A. 2006, AAN, 339, 1
Puebla, R. E., Diaz, M. P., & Hubeny, I. 2007, AJ, 134, 1923
Rappaport, S., Joss, P. C., & Webbink, R. F. 1982, ApJ, 254, 616
Rappaport, S., Verbunt, F., & Joss, P. C. 1983, ApJ, 275, 713
Richter, G. A. 1961, Veröff. Sternw. Sonneberg, 4, 433
Richter, G. A., Notni, P., & Tiersch, H. 1988, Astron. Nachr., 309, 91
Ringwald, R. A. 1994, in ASP Conf. Ser. 56, Interacting Binary Stars, ed. A. W. Shafter (San Francisco, CA: ASP), 294
Ritter, H., & Kolb, U. 2003, A&A, 404, 301
Robinson, E. L. 1976, ARA&A, 14, 119
Rosen, S. R., et al. 2001, MNRAS, 322, 631
Schenker, K., Kolb, U., & Ritter, H. 1998, MNRAS, 297, 633
Schlegel, D. J., Finkbeiner, D. P., & Davis, M. 1998, ApJ, 500, 525
Schwope, A. D., Hambarayan, V., Schwarz, R., Kanbach, G., & Gänsicke, B. T. 2002, A&A, 392, 541
Sepinsky, J. F., Sion, E. M., Szkody, P., & Gänsicke, B. T. 2002, ApJ, 574, 937
Shakura, N. I., & Sunyaev, R. A. 1973, A&A, 24, 337
Sheets, H. A., Thorstensen, J. R., Peters, C. J., Kapusta, A. B., & Taylor, C. J. 2007, PASP, 119, 494
Sion, E. M. 1991, AJ, 102, 295
Sion, E. M., Cheng, F. H., Szkody, P., Sparks, W., Gänsicke, B. T., Huang, M., & Mattei, J. 1998, ApJ, 496, 449
Sion, E. M., Gänsicke, B. T., Long, K. S., Szkody, P., Knigge, C., Hubeny, I., de Martino, D., & Godon, P. 2008, ApJ, 681, 543
Sion, E. M., Godon, P., Cheng, F., & Szkody, P. 2007, AJ, 134, 886
Sion, E. M., Szkody, P., Cheng, F., Gänsicke, B. T., & Howell, S. B. 2003, ApJ, 583, 907
Sion, E. M., Szkody, P., Gänsicke, B. T., Cheng, F. H., LaDous, C., & Hassall, B. 2001, ApJ, 555, 834
Spruit, H. C., & Ritter, H. 1983, A&A, 124, 267
Spruit, H. C., & Taam, R. E. 2001, ApJ, 548, 900
Szkody, P., Gänsicke, B. T., Howell, S. B., & Sion, E. M. 2002a, ApJ, 575, L79
Szkody, P., Gänsicke, B. T., Sion, E. M., Howell, S. B., & Cheng, F. H. 2003, A&A, 126, 1451
Szkody, P., Sion, E. M., Gänsicke, B. T., & Howell, S. B. 2002b, in ASP Conf. Ser. 261, The Physics of Cataclysmic Variables and Related Objects, ed. B. T. Gänsicke, K. Beuermann, & K. Reinsch (San Francisco, CA: ASP), 21
Taam, R. E., Sandquist, E. L., & Dubus, G. 2003, ApJ, 592, 1124
Taam, R. E., & Spruit, H. C. 2001, ApJ, 561, 329
Taylor, C. J., & Thorstensen, J. R. 1996, PASP, 108, 894
Townsley, D., & Bildsten, L. 2003, ApJ, 596, L227
Townsley, D., & Bildsten, L. 2004, ApJ, 600, 390
Townsley, D., & Gänsicke, B. T. 2009, ApJ, 693, 1007
Urban, J. A., & Sion, E. M. 2006, ApJ, 642, 1029
Verbunt, F., & Zwaan, C. 1981, A&A, 100, L7
Vogt, N., & Bateson, F. M. 1982, A&AS, 48, 383
Wade, R. A., & Hubeny, I. 1998, ApJ, 509, 350
Warner, B. 1987, MNRAS, 227, 23
Warner, B. 1995, Cataclysmic Variable Stars (Cambridge: Cambridge Univ. Press)
Webbink, R. F. 1981, BAAS, 12, 848
Weber, E. J., & Davis, L. 1967, ApJ, 148, 217
Whyte, C. A., & Eggleton, P. P. 1980, MNRAS, 190, 801
Wood, M. A. 1995, in White Dwarfs, Proceedings of the 9th European Workshop on White Dwarfs, Lecture Notes in Physics 442, ed. Detlev Koester & Klaus Werner (Berlin: Springer), 41
Woudt, P. A., Warner, B., & Spark, M. 2005, MNRAS, 364, 107